

A NUMERICAL METHOD FOR COUPLING THE BGK MODEL AND EULER EQUATION THROUGH THE LINEARIZED KNUDSEN LAYER

HONGXU CHEN, QIN LI, AND JIANFENG LU

ABSTRACT. The Bhatnagar-Gross-Krook (BGK) model, a simplification of the Boltzmann equation, in the absence of boundary effect, converges to the Euler equation when the Knudsen number is small. In practice, however, Knudsen layers emerge at the physical boundary, or at the interfaces between the two regimes. We model the Knudsen layer using a half-space kinetic equation, and apply a half-space numerical solver [29, 30] to quantify the transition between the kinetic to the fluid regime. A full domain numerical solver is developed based on domain-decomposition method, with the Euler solver and kinetic solver applied on the appropriate parts of the domain and connected through the half-space solver.

1. INTRODUCTION

The Boltzmann equation is a model equation in kinetic theory. It is a standard equation that describes the dynamics of rarified gas particles on the phase plane, and is extensively used in aerospace engineering, nuclear engineering and many other fields. In the dimensionless form the equation reads

$$(1) \quad \partial_t F + v \cdot \nabla_x F = \frac{1}{\varepsilon} Q(F, F), \quad (t, x, v) \in \mathbb{R}^+ \times \mathbb{R}^d \times \mathbb{R}^d,$$

where $F = F(t, x, v)$ is the density function of the particles at time $t \in \mathbb{R}^+$, position and velocity (x, v) in the phase space. In the equation, d is the spatial dimension, and $\varepsilon > 0$ is the Knudsen number given by the ratio of the mean free path and the characteristic domain length scale. The general form of the collision operator is:

$$(2) \quad Q(F, F) = \int_{\mathbb{R}^d} \int_{\mathbb{S}^{d-1}} B(v, v_*, \sigma) [F(v')F(v'_*) - F(v)F(v_*)] d\sigma dv_*,$$

and it describes the probability of two particles with velocity v and v_* colliding each other and resulting in velocity (v', v'_*) afterwards. We only consider elastic collision and thus the pre and after collision velocity satisfy the momentum and energy conservation:

$$v' = \frac{v + v_*}{2} + \frac{|v - v_*|}{2} \sigma; \quad v'_* = \frac{v + v_*}{2} - \frac{|v - v_*|}{2} \sigma,$$

with the vector σ varying on the unit sphere. The collision kernel B is a non-negative function of the form $B(v, v_*, \sigma) = B(|v - v_*|, \cos \theta)$ with $\theta = \arccos \left(\frac{\sigma \cdot (v - v_*)}{|v - v_*|} \right)$ being the deviation angle.

Date: June 18, 2022.

The work of H.C. and Q.L. is supported in part by National Science Foundation under the grant DMS-1619778. The work of J.L. is supported in part by the National Science Foundation under the grant DMS-1415939. The collaboration is also supported by National Science Foundation through KI-Net under grants RNMS-1107291 and RNMS-1107444. We thank Weiran Sun for helpful discussions.

The Euler equations are a set of equations for describing fluid dynamics. They are used to characterize the motion of the perfect fluid without viscosity that conserve mass, momentum and energy. The compressible Euler equations read:

$$(3) \quad \begin{cases} \partial_t \rho + \nabla_x \cdot (\rho u) = 0; \\ \partial_t (\rho u) + \nabla_x (\rho u \otimes u + \rho T) = 0; \\ \partial_t E + \nabla_x \cdot ((E + \rho T)u) = 0, \end{cases}$$

where E is the energy density given by

$$E = \frac{1}{2} \rho u^2 + \frac{d}{2} \rho T.$$

The two sets of equations are derived from statistical mechanics and fluid dynamics respectively. However, it was shown in [2] that the two sets of equations are equivalent in the zero limit of the Knudsen number ε . Indeed, in the small ε regime, the collision term becomes extremely stiff, and the intensive collisions between particles quickly drive the system to local “equilibrium” state. Such state is termed “Maxwellian”, obtained by setting $Q(F, F) = 0$, and this gives a Gaussian form:

$$(4) \quad F(t, x, v) \xrightarrow{\varepsilon \rightarrow 0} M[F](t, x, v) = \frac{\rho(t, x)}{[2\pi T(t, x)]^{d/2}} \exp\left(-\frac{(v - u(t, x))^2}{2T(t, x)}\right).$$

where the three physical quantities ρ , u and T in the Maxwellian are determined by the moments of F , namely:

$$(5) \quad \begin{pmatrix} \rho(x, t) \\ \rho(x, t)u(x, t) \\ d\rho(x, t)T(x, t) \end{pmatrix} = \int_{\mathbb{R}^d} F(x, v, t) \begin{pmatrix} 1 \\ v \\ |v - u|^2 \end{pmatrix} dv.$$

Via Chapman-Enskog expansion, as shown in [2], in the leading order, one can show that these quantities satisfy the Euler equation (3).

Computing the Boltzmann equation (1) accurately and efficiently is a long standing challenging problem. It is specially difficult in the fluid regime when the equation is asymptotically equivalent to the Euler equations. Besides the standard difficulties is brought by the complicated integration form of the collision term Q , the high dimensionality, another immediate challenge comes from numerical stability restriction. The nonlinear nature of the collision term (2) prevents efficient implicit solvers, but all explicit solvers have to satisfy the severe stability condition, meaning:

$$(6) \quad \Delta t \ll \varepsilon.$$

In the fluid regime, $\varepsilon \rightarrow 0$, and the numerical algorithms tend to be extremely expensive.

There are mainly two approaches to overcome this stability restriction. The first approach taken to overcome this stability restriction is to design asymptotic preserving scheme. “Asymptotic preserving” (AP), as a concept, was termed in [21] for general kinetic equations with stiff terms, although the earliest AP method appeared one decade earlier for neutron transport equation [25]. If a numerical solver can produce a numerical solution explicitly without satisfying the CFL condition (6), it is called “AP” method. In the context of kinetic equations, and the Boltzmann equation specifically, an AP method is a numerical

solver that is able to capture the fluid limit without using fine grid (6). For (nonlinear) Boltzmann equation, the first AP algorithm was proposed by Jin and Filbet in [16]. Li and Pareschi [27] followed the Wild sum idea [14, 31] and designed a series of scheme that achieves arbitrary high order in both space and time. The micro-macro decomposition method was developed in [4] that separates the stiff terms. A summary on AP method for kinetic equations are found in [22], and then [15] for plasma computation. Different AP methods achieve AP property via different techniques, but a common theme they share is that they all heavily depend on the analytical understanding of the equation: an Euler solver is implanted in the kinetic scheme, and as $\varepsilon \rightarrow 0$, the weight on the Euler solver becomes dominant, driving the numerical solution to that of the Euler equations.

There are two main assumptions that all these AP methods rely on. 1: the domain is assumed to be infinitely big, or for bounded domain, the boundary condition is periodic, so that there are no physical boundary layer induced close to the wall; 2. ε stays close to a constant and changes slowly, so that interior layers induced by the drastic change of ε can be avoided. Both assumptions are aimed at eliminating boundary layers, a physical phenomenon that is still mostly unknown. Indeed, in both scenarios: injecting particles (imposing inflow boundary conditions) at the wall, and changing the mean-free-path in a small domain, could bring drastic changes to the distribution function F . These changes usually take place within a small region of size $\mathcal{O}(\varepsilon)$. The complete analysis for the boundary layer behavior is still out of reach, especially in the fully nonlinear case. The brute-force computation [1] shows very complicated solution behavior and sophisticated constraints need to be imposed on macroscopic quantities for the equation to be wellposed. While the theoretical justification for this phenomenon is completely open, the numerical study is prohibitively expensive as well: to capture sharp transition, very fine discretization that resolves the layers are absolutely necessary.

These bring us to the second approach, which is called the domain decomposition, where one treats different regions separately and then couple them together through the interface. In particular, for the Boltzmann equation and Euler equation, the idea that at the leading order, inside the boundary layer the kinetic equation satisfies a closed system. If we are able solve the leading order kinetic equation in the boundary layer, we can use the solution from the kinetic regime as the incoming data for the fluid regime. Then we approximate the kinetic equation in the fluid regime using the same method for the pure fluid equation.

Advancements have been made in the linearized setting both analytically and numerically in the recent years. On the analytical side, mathematical studies of the Knudsen layer behavior started attracting attention long time ago. It was modeled as a half-space-problem in the pioneer paper [5], and a decade later, in the seminal paper [8] the authors studied the wellposedness of the half-space equation of the linearized Boltzmann equation, and showed that the uniqueness requires an extra condition which depends on the limiting Mach number. The results they obtained greatly generalized the results obtained in [3] where Mach number is assumed to be 0 (also termed Milne problem).

The numerical study of the half-space equation was a much recent topic. There are several obvious difficulties. If one models the boundary layers using half-space equations: the equation is supported in the half spatial domain that is infinitely big. How to discretize an infinitely big domain is an immediate problem. Besides, the wellposedness results from [8] requires a very special condition that is numerically

hard to interpret. Despite these difficulties, several attempts were still made [11, 23, 17, 7], and some methods do present to be quite effective. However, all methods rely on strong physical intuitions that could be mathematically hard to justify.

A numerically accessible and justifiable scheme was finally developed in [29]. In the paper, the authors used damping-recovering technique, and by studying the spectrum of the damped equation, a spectral-type method was developed that achieves spectral accuracy in v and is analytical in x . This method does not rely on the truncation in the spacial domain, and thus no extra error is introduced. What is more, the numerical method is constructive and the uniqueness is obtained automatically: this allows us to avoid the special decomposition of the solution space as suggested in [8].

This successful numerical treatment of the half-space equation allows the author of [29] to approximate the linear transport equation by diffusion equation in [28]. It also allows us to deal with the Boltzmann system where the Knudsen layer occurs, either at both the physical boundaries, and at the interface where sharp transition of ε takes place. This is indeed the aim of the current paper. We perform domain decomposition, and apply the Euler solver and kinetic solver on the appropriate parts of the domain which are connected through the half-space solver that provide a numerical solution to the Knudsen layer.

Here we also mention other domain decomposition approach. In [10, 12, 13], the author use the buffer zone to achieve a smooth transition to connect the fluid and kinetic regime. In [18, 19, 26], the H -function or generalized H - functions are used to study the boundary layer equation. In [24], where the corresponding boundary layer equation is solved by iterating incorporated with Chapman-Enskog expansion [20]. And in [6], the author approximate the half-space problem to provide the boundary condition for the fluid regime in a finite volume framework.

The paper is laid out as follows. Since the computation of the Knudsen layer is the main ingredient in the entire scheme, we first review it in Section 2. Section 3 and 4 are devoted to linearized and nonlinear setting of the coupling between the Knudsen layer computation and the AP solver used for regions without layers. Numerical evidence will be demonstrated in Section 5.

2. LINEARIZED SYSTEMS AND THE KNUDSEN LAYER

We describe background of the problem in this section. Mainly, in Section 2.1, we will describe the Boltzmann equation and its BGK model, its hydrodynamic Euler limit, the linearization and the linearized Euler limit (termed acoustic limit). We then give an overview of the theory and the numerical methods for the Knudsen layer equation in Section 2.2.

2.1. Linearized BGK equation and its fluid limit. The BGK model is a simplified model for the Boltzmann equation, and it reads:

$$(7) \quad \partial_t F + v \cdot \nabla_x F = \frac{1}{\varepsilon} (M[F] - F), \quad (t, x, v) \in \mathbb{R}^+ \times \mathbb{R}^d \times \mathbb{R}^d,$$

where the collision Q in (1) is replaced by the BGK operator. Here $M[F]$ is a Maxwellian distribution (local equilibrium) depending on F , given by

$$(8) \quad M[F] = \frac{\rho}{(2\pi T)^{d/2}} \exp\left(-\frac{(v-u)^2}{2T}\right),$$

with the macroscopic quantities ρ , u and T obtained from the moments of F (5). Such definition enforces the Maxwellian to share the first moments with F , meaning:

$$\int \phi(v)(M[F] - F)dv = 0,$$

with $\phi(v) = 1, v$ or v^2 .

When the system is near global equilibrium, the linearized BGK equation is obtained by expanding F around the given global Maxwellian. Suppose the global Maxwellian has its macroscopic state (ρ_*, u_*, T_*) (independent of x), we then can expand F around M_* :

$$(9) \quad F = M_* + \sqrt{M_*}f, \quad \text{with} \quad M_* = \frac{\rho_*}{(2\pi T_*)^{d/2}} \exp\left(-\frac{|v - u_*|^2}{2T_*}\right),$$

and substitute it in the BGK equation (7). Keeping the first order expansion, the linearized BGK equation is obtained:

$$(10) \quad \partial_t f + v \cdot \nabla_x f = \frac{1}{\varepsilon} \mathcal{L}_* f, \quad \text{with} \quad \mathcal{L}_* f = m_*[f] - f.$$

Similar to the BGK equation, the linear Maxwellian $m_*[f](v)$ is a quadratic function, defined so that it preserves the first $d + 2$ moments of f , when weighted by $\sqrt{M_*}$, meaning:

$$(11) \quad \langle f - m_*[f], v^k \rangle_{M_*} = \int_{\mathbb{R}} (f - m_*[f]) v^k \sqrt{M_*} dv = 0, \quad k = 0, 1, 2.$$

In the equation we used the notation (considering f contains $\sqrt{M_*}$ already):

$$(12) \quad \langle f, g \rangle_{M_*} = \int f g \sqrt{M_*} dv.$$

In 1D, we define the moments $(\tilde{\rho}, \tilde{u}, \tilde{T})$ of f by

$$(13) \quad \begin{pmatrix} \tilde{\rho} \\ \tilde{\rho} u_* + \rho_* \tilde{u} \\ \tilde{\rho}(u_*^2 + T_*) + 2\rho_* u_* \tilde{u} + \rho_* \end{pmatrix} = \int_{\mathbb{R}} f \begin{pmatrix} 1 \\ v \\ v^2 \end{pmatrix} \sqrt{M_*} dv = \langle f, \begin{pmatrix} 1 \\ v \\ v^2 \end{pmatrix} \rangle_{M_*},$$

then we can explicitly express $m_*(v)$ to be:

$$(14) \quad m_*[f](v) = \left[\frac{\tilde{\rho}}{\rho_*} + \frac{\tilde{u}}{T_*}(v - u_*) + \frac{\tilde{T}}{2T_*} \left(\frac{(v - u_*)^2}{T_*} - 1 \right) \right] \sqrt{M_*}.$$

Similar to the nonlinear case, the linearized BGK model also has its corresponding fluid limit. In the zero limit of ε , the linearized distribution profile f is asymptotically equivalent to $m_*[f]$, and equation (10) converges to the limiting acoustic equation:

$$(15) \quad \partial_t U + \mathbf{A} \cdot \partial_x U = 0,$$

where

$$\mathbf{A} = \begin{pmatrix} u_* & \rho_* & 0 \\ \frac{T_*}{\rho_*} & u_* & 1 \\ 0 & 2T_* & u_* \end{pmatrix}, \quad \text{and} \quad U = \begin{pmatrix} \tilde{\rho} \\ \tilde{u} \\ \tilde{T} \end{pmatrix}.$$

Remark 1. We note that this set of equation could also be obtained by directly linearizing the nonlinear Euler equation (3) around the reference state (ρ_*, u_*, T_*) . This means that the two procedures – linearizing the BGK equation and taking the hydrodynamic limit – commute.

Equation set (15) is a hyperbolic system, and the treatment is standard. We diagonalize the system by setting $A = V \cdot D \cdot V^{-1}$ for:

$$(16) \quad \partial_t U + V \cdot D \cdot V^{-1} \cdot \partial_x U = 0 \quad \implies \quad \partial_t \eta + D \cdot \partial_x \eta = 0,$$

where

$$(17) \quad \eta = V^{-1} \cdot U = \begin{pmatrix} \frac{T_*}{\rho_*} \tilde{\rho} - \frac{\tilde{T}}{2} \\ \frac{\tilde{p}}{\rho_*} + \sqrt{\frac{3}{T_*}} \tilde{u} + \frac{\tilde{T}}{T_*} \\ \frac{\tilde{p}}{\rho_*} - \sqrt{\frac{3}{T_*}} \tilde{u} + \frac{\tilde{T}}{T_*} \end{pmatrix}, \quad \text{and} \quad D = \text{diag}(u_*, u_* + \sqrt{3T_*}, u_* - \sqrt{3T_*}).$$

This formulation gives a clear picture of the evolution of the system: η_i satisfies the advection equation with speed $d_i = D_{ii}$ (for $i = 1, 2, 3$):

$$(18) \quad \partial_t \eta_i + d_i \partial_x \eta_i = 0.$$

In fact, η_i , obtained through linear transformation on the macroscopic scale, also has microscopic interpretation: it can be obtained by projecting f onto the following polynomials:

$$(19) \quad \eta_i = \langle f, p_i \rangle_{M_*},$$

where

$$\begin{cases} p_1 = -\frac{1}{2\rho_*}(v - u_*)^2 + \frac{3T_*}{2\rho_*} \\ p_2 = \frac{1}{\rho_* T_*}(v - u_*)^2 + \frac{1}{\rho_*} \sqrt{\frac{3}{T_*}}(v - u_*) \\ p_3 = \frac{1}{\rho_* T_*}(v - u_*)^2 - \frac{1}{\rho_*} \sqrt{\frac{3}{T_*}}(v - u_*) \end{cases}.$$

We conclude without proof here that in the zero limit of ε , without boundary effect, $f \rightarrow m_*[f]$ whose macroscopic quantities satisfy the acoustic advection equation (17). The assumption $f \rightarrow m_*[f]$ is rather strong, without which, the moment equation cannot be closed.

However, this assumption indeed doesn't hold close to the physical boundary, or at the interface where ε drastically changes in its magnitude. In both cases, a boundary layer would emerge. The layer is of size of $\mathcal{O}(\varepsilon)$, and within the layer, f largely depends on the initial and boundary conditions, which can be significantly different from $m_*[f]$, the linear Maxwellian. Therefore in the layer, the fluid equation is not a good approximation. A layer equation is added to describe such transition, which we will discuss in depth in the next subsection.

2.2. Half-space kinetic boundary layer equation. The Knudsen layer equation, or the half-space equation, was initially proposed to describe the Knudsen layer in an early work [5], in which the authors proposed to approximate the curved boundary using the tangent plane at each boundary point, and the coordinates along the orthogonal direction are “stretched” to “zoom-in” the layer behavior. The terms in

the BGK equation are then re-balanced to reflect the strength of the terms, resulting the layer equation that is supported on half domain.

We use the following 1D equation with $x \in [0, 1]$ with inflow boundary condition as an example. The presentation here largely follows the previous works [29, 30]. The equation reads:

$$(20) \quad \begin{cases} \partial_t f + v \partial_x f = \frac{1}{\varepsilon} \mathcal{L}_* f = \frac{1}{\varepsilon} (m_*[f] - f), & (t, x, v) \in \mathbb{R}^+ \times [0, 1] \times \mathbb{R}, \quad \varepsilon \ll 1 \\ f(t = 0, x, v) = f_0(x, v) \\ f(t, x = 0, v) = \phi_l(t, v), & v > 0 \\ f(t, x = 1, v) = \phi_r(v, t), & v < 0 \end{cases} .$$

Remark 2. Note that inflow boundary condition is different from Dirichlet type condition: at the left end $x = 0$, we provide flow that only propagates to the right ($v > 0$) and at the right end we provide inflow data for $v < 0$.

At the two physical boundaries $x = 0$ and $x = 1$, layers of width of $\mathcal{O}(\varepsilon)$ appear. For all fixed $[a, b] \subset (0, 1)$, with ε significantly small, the boundary layers are then included in $(0, a]$ and $[b, 1)$, and the acoustic limit is achieved in the interior $[a, b]$.

Let us focus on the boundary layer near $x = 0$ first. To understand the layer structure, we first define a new variable $z = \frac{x}{\varepsilon}$. Using the blow-up variable z , the equation is rescaled to

$$\partial_t f + \frac{v}{\varepsilon} \partial_z f = \frac{1}{\varepsilon} \mathcal{L}_* f .$$

The leading order is of $\mathcal{O}(\frac{1}{\varepsilon})$ and it balances the transport term and the collision operator. We now can write our Knudsen layer equation for all t :

$$(21) \quad \begin{cases} v \partial_z f = \mathcal{L}_* f, & (z, v) \in \mathbb{R}^+ \times \mathbb{R} \\ f|_{z=x=0} = \phi_l(v; t), & v > 0 \end{cases} .$$

where t is a parameter involved in the equation through the boundary condition. Now the left inflow condition becomes the inflow condition for (21) imposed at $z = 0$. For arbitrary fixed $x \neq 0$, in the zero limit of ε , $z = \frac{x}{\varepsilon} \rightarrow \infty$, meaning that the solution of the layer equation, when confined at $z = \infty$, is mapped to the interior.

The same derivation is done for the right boundary, with $z = \frac{1-x}{\varepsilon}$ and $\tilde{v} = -v$. A similar half-space equation is obtained:

$$\tilde{v} \partial_z f = \mathcal{L}_* f, \quad f|_{z=0} = \phi_r(-v), \quad v > 0 .$$

with the inflow data coming from the right boundary condition from the original equation (20).

In the rest of this section we summarize the results obtained for the layer equation (21), including the wellposedness result, and a spectral method designed to solve the half-space equation. The algorithm was developed in [29, 30]. For the conciseness of the notation, we also drop the lower index l .

2.2.1. *Wellposedness.* For the wellposedness we cite the following:

Theorem 1 (Theorem 1 from [8] and Theorem 3 from [29]). *Let the incoming data $\phi \in L^2((1+|v|)\mathbf{1}_{v>0}dv)$, the half-space equation*

$$(22) \quad \begin{cases} v\partial_z f = \mathcal{L}_* f, & (z, v) \in \mathbb{R}^+ \times \mathbb{R} \\ f|_{z=0} = \phi(v), & v > 0 \end{cases}$$

has a unique solution such that

$$(23) \quad \lim_{z \rightarrow \infty} f(z, \cdot) \in H^+ \oplus H^0.$$

Here H^+ and H^0 are the collections of positive and zero modes associated with multiplicative operator v in $\text{Null}\mathcal{L}_*$, the null space of the collision operation \mathcal{L}_* .

The theorem is proved for general kinetic equations, and the definitions of $H^{+,0}$ are rather vague. In some cases, these spaces could be made more explicit. One example is the linearized BGK equation.

Consider the explicit form given in (14), m_* has a quadratic function form, so setting $\mathcal{L}_*[f] = 0$ naturally leads to the fact that f is also a quadratic function. This means:

$$(24) \quad \text{Null}\mathcal{L}_* = \text{span}\{\sqrt{M_*}, v\sqrt{M_*}, v^2\sqrt{M_*}\}.$$

Recall that H^+ and H^0 are eigensubspace of the multiplicative operator v restricted on $\text{Null}\mathcal{L}_*$, then with further calculation we are also able to obtain them explicitly:

$$(25) \quad \begin{cases} \chi_0(v) = \frac{1}{\sqrt{6\rho_*}} \left(\frac{(v-u_*)^2}{T_*} - 3 \right) \sqrt{M_*}; \\ \chi_+(v) = \frac{1}{\sqrt{6\rho_*}} \left(\sqrt{\frac{3}{T_*}}(v-u_*) + \frac{(v-u_*)^2}{T_*} \right) \sqrt{M_*}; \\ \chi_-(v) = \frac{1}{\sqrt{6\rho_*}} \left(\sqrt{\frac{3}{T_*}}(v-u_*) - \frac{(v-u_*)^2}{T_*} \right) \sqrt{M_*}. \end{cases}$$

These functions satisfy

1. they expand the null space and form an orthogonal basis: $\text{Null}\mathcal{L}_* = \text{span}\{\chi_0, \chi_+, \chi_-\}$ and $\langle \chi_i, \chi_j \rangle = \delta_{ij}$ for all $i, j \in \{0, +, -\}$:

$$\int \chi_i(v)\chi_j(v)dv = \langle \chi_i, \chi_j \rangle = \delta_{ij};$$

2. they are eigenfunctions of the multiplicative operator v restricted in $\text{Null}\mathcal{L}_*$:

$$\langle v\chi_i, \chi_j \rangle = u_i\delta_{ij}$$

3. for all $i, j \in \{0, -, +\}$. The eigenvalues u_i are given by the bulk velocity and the temperature:

$$(26) \quad u_0 = u_*, \quad u_+ = u_* + \sqrt{3T_*}, \quad u_- = u_* - \sqrt{3T_*}.$$

The eigensubspace is then given by

$$H^+ = \text{span}\{\chi_i | u_i > 0\}, \quad H^- = \text{span}\{\chi_i | u_i < 0\}, \quad \text{and} \quad H^0 = \text{span}\{\chi_i | u_i = 0\},$$

where $i \in \{+, -, 0\}$, so $\text{Null}\mathcal{L}_* = H^+ \oplus H^0 \oplus H^-$. For convenience of the notation, we now define the dimension of the spaces:

$$\nu_{\pm,0} = \dim H^{\pm,0},$$

and re-label the modes in each space:

$$(27) \quad H^\pm = \text{span}\{\zeta_{\pm,1}, \dots, \zeta_{\pm,\nu_\pm}\}, \quad H^0 = \text{span}\{\zeta_{0,1}, \dots, \zeta_{0,\nu_0}\}.$$

According to Theorem 1, for uniqueness, at $z = \infty$, the solution has to be in:

$$\text{span}\{\zeta_{0,1}, \dots, \zeta_{0,\nu_0}, \zeta_{+,1}, \dots, \zeta_{+,\nu_+}\} = \text{span}\{\chi_i | u_i \geq 0\}.$$

Remark 3. We note that the theorem discusses the uniqueness and asserts that the projection of $f|_{z=\infty}$ on H^- should be zero. If we remove this requirement, the equation loses its uniqueness but we still have the existence. In fact, one can show there are infinitely many solutions. The solution space is simply:

$$f^l + H^-$$

where f^l is the unique solution in Theorem 1.

2.2.2. Spectral method for half-space equations. Finding the numerical solution to the half-space problem, however, carries a different challenging aspect. The problem is supported on an infinite domain, which cannot be numerically handled easily, and the theorem only states the uniqueness under certain constraints, but the constraints are rather abstract.

In [29], a semi-analytic spectral method was developed that achieves quasi-optimality in v and is analytic in x . The algorithm relies on the damping-recovering idea. To be more specific, a damping term is introduced and added to the right hand side of the equation, so that all elements in $\text{Null}\mathcal{L}_*$ are damped out from the solution, forcing the solution to the damped equation, denoted by f_d , to be zero at $z = \infty$. The trick of finding the solution to the original equation lies in the fact that a very special boundary condition can be designed, so that when it is put into the damped equation, it cancels the effect of the damping term.

To make the paper self-contained, let us briefly recall the algorithm below. The damped half-space equation reads:

$$(28) \quad \begin{cases} v\partial_z f_d = \mathcal{L}_d f_d; \\ f_d(z=0, v) = \phi(v), \quad v > 0; \\ \lim_{z \rightarrow \infty} f_d(z, \cdot) = 0. \end{cases}$$

where the damped collision term reads:

$$\begin{aligned} \mathcal{L}_d f = \mathcal{L}_* f + & \sum_{i \in \{+, -, 0\}} \sum_{j=1}^{\nu_i} \alpha(v + u_*) \zeta_{i,j} \langle v \zeta_{i,j}, f \rangle \\ & + \sum_{i=1}^{\nu_0} \alpha(v + u_*) \mathcal{L}^{-1}((v + u_*) \zeta_{0,j}) \langle v \mathcal{L}^{-1}((v + u_*) \zeta_{0,j}), f \rangle. \end{aligned}$$

Here α is some small number and its value does not affect the results. The recovering formula is summarized in the following theorem.

Theorem 2 (Proposition 3.4 from [29]). *Let $\phi \in L^2((1 + |v|)\mathbf{1}_{v>0}dv)$, then*

$$(29) \quad f = f_d - \sum_{i=1}^{\nu_+} \xi_{+,i}(g_{+,i} - \zeta_{+,i}) - \sum_{j=1}^{\nu_0} \xi_{0,j}(g_{0,j} - \zeta_{0,j})$$

uniquely solves (21) with $\lim_{z \rightarrow \infty} f = f_\infty \in H^+ \oplus H^0$ is the end-state given by

$$(30) \quad f_\infty = \sum_{j=1}^{\nu_+} \xi_{+,j} \zeta_{+,j} + \sum_{k=1}^{\nu_0} \xi_{0,k} \zeta_{0,k} = \sum_{j=1}^{\nu_+} \langle f_\infty, \zeta_{+,j} \rangle \zeta_{+,j} + \sum_{k=1}^{\nu_0} \langle f_\infty, \zeta_{0,k} \rangle \zeta_{0,k}.$$

Here f_d solves (28) with inflow data ϕ , and $g_{i,j}$ solves (28) with inflow data $\zeta_{i,j}$. $\{\xi_{+,j}, \xi_{0,k}\}$ are coefficients that solve:

$$C \cdot \vec{\xi} = \vec{Q}, \quad \text{with } C = \begin{pmatrix} C_{++}, C_{+0} \\ C_{0+}, C_{00} \end{pmatrix}, \quad \vec{\xi} = \begin{pmatrix} \vec{\xi}_+ \\ \vec{\xi}_0 \end{pmatrix}, \quad \text{and } \vec{Q} = \begin{pmatrix} \vec{Q}_+ \\ \vec{Q}_0 \end{pmatrix}.$$

The vector coefficient $\vec{\xi}_+ = [\xi_{+,1}, \xi_{+,2}, \dots, \xi_{+,\nu_+}]^T$, and $\vec{Q}_+ = [\langle v\zeta_{+,1}, f_d \rangle, \dots, \langle v\zeta_{+,\nu_+}, f_d \rangle]^T$ (and similarly for $\vec{\xi}_0$ and \vec{Q}_0). The matrix is defined by:

$$C_{++,ij} = \langle v\zeta_{+,i}, g_{+,j}|_{z=0} \rangle, \quad C_{+0,ij} = \langle v\zeta_{+,i}, g_{0,j}|_{z=0} \rangle, \\ C_{0+,ij} = \langle v\zeta_{0,i}, g_{+,j}|_{z=0} \rangle, \quad C_{00,ij} = \langle v\zeta_{0,i}, g_{0,j}|_{z=0} \rangle.$$

The theorem suggests the following steps to compute f :

1. compute the damped equation (28) for f_d and $g_{i,j}$ using different boundary conditions;
2. use $g_{i,j}$ to define the matrices C and use f_d to define \vec{Q} for computing $\vec{\xi}$;
3. assemble f according to (29) and $f|_{z=\infty}$ according to (30).

The details of the algorithm that computes the damped equation (28) are summarized in Appendix.

3. ACOUSTIC LIMIT OF THE LINEARIZED BGK EQUATION WITH KINETIC BOUNDARY CONDITION

Knudsen layers emerge in two scenarios: 1. the whole domain is in fluid regime and the Knudsen layer emerges only at the physical boundaries; 2. part of the domain is governed by fluid regime while the other part is in kinetic regime; if so, boundary layers emerge both at the interface between the two regions and at the physical boundary. We discuss the first scenario in this section, and leave the second scenario to Section 4.

Without loss of generality, we assume that the spatial domain is $[0, 1]$, the linearized BGK system is presented in (20), repeated here for convenience:

$$(31) \quad \begin{cases} \partial_t f + v\partial_x f = \frac{1}{\varepsilon} \mathcal{L}_* f = \frac{1}{\varepsilon} (m_* - f), & (t, x, v) \in \mathbb{R}^+ \times [0, 1] \times \mathbb{R}, \quad \varepsilon \ll 1 \\ f(t = 0, x, v) = f_0(x, v) \\ f(t, x = 0, v) = \phi_l(t, v), & v > 0 \\ f(t, x = 1, v) = \phi_r(v, t), & v < 0 \end{cases}.$$

As $\varepsilon \rightarrow 0$, for any interior domain $[a, b] \subsetneq [0, 1]$, this equation is well approximated by the linearized Euler equation and its diagonalization:

$$(32) \quad \partial_t U + \mathbf{A} \cdot \partial_x U = 0, \quad \Rightarrow \quad \partial_t \eta_i + d_i \partial_x \eta_i = 0.$$

Depending on the sign of d_i , η_i is either advecting left or right. We here point out two connections between the fluid limit and the boundary layer solution, from macro and micro perspectives respectively.

- The speed d_i are counterparts of the “averaged speed” of $\zeta_{\pm/0}$ defined in (27), namely (with an arbitrary ordering)

$$d_1 = u_0 = u_*, \quad d_2 = u_+ = u_* + \sqrt{3T_*}, \quad d_3 = u_- = u_* - \sqrt{3T_*}.$$

- The projection of $f|_{z=\infty}$ on ζ , denoted as ξ as in Theorem 2, is a counterpart of η . If we compare the definition of η in (19) and $\chi_{0,\pm}$ in (25), we see that:

$$\chi_0 = -\frac{2\sqrt{\rho_*M_*}}{\sqrt{6T_*}}p_1, \quad \chi_+ = \frac{\sqrt{\rho_*M_*}}{\sqrt{6}}p_2, \quad \chi_- = \frac{\sqrt{\rho_*M_*}}{\sqrt{6}}p_3.$$

and thus ζ s, the re-labels of χ s are ps multiplied by constants, meaning $\xi = \langle f, \zeta \rangle$ and $\eta = \langle f, p \rangle_{M_*}$ are counterparts of each other, with the specific matching determined by the Mach number.

Remark 4. Note that u_+ has a positive sign as the subscript but it does not mean $u_+ > 0$. Its value is determined by Mach number. For example, if Mach number is smaller than -1 , then $u_+ = u_* + \sqrt{3T_*} < 0$.

Of course this connection is not a coincidence. Actually this is crucial for correctly imposing the boundary conditions for the hyperbolic system such that the resulting equation is well-posed. On the left boundary, we impose Dirichlet data only for the modes that are propagating to the right, meaning we need a value for η_i at $x = 0$ if $d_i > 0$. This value should come from kinetic boundary condition, and is expected to be computable through the half-space equation. Indeed, as asserted by the theorem, the projection of $f|_{z=\infty}$ on H^+ is uniquely determined, meaning $\xi_{+,j} = \langle f, \zeta_{+,j} \rangle$ is obtainable from ϕ . Such matched one-to-one correspondence enables the coupling between the linearized Euler equation with the kinetic boundary data.

Below we assume the Mach number is between 0 and 1 for the simplicity of presentation, that is $u_* + \sqrt{3T_*} > u_* > 0$ while $u_* - \sqrt{3T_*} < 0$. In this case, in the fluid regime, η_1 and η_2 are right-moving modes calling for boundary condition at $x = 0$, while η_3 is the left-moving mode calling for boundary condition at $x = 1$. The method works similarly for other cases of Mach number with straightforward changes.

Discretize the domain into N equal cells with cell length $h = \frac{1}{N}$:

$$0 = x_0 < x_1 < x_2 < \cdots < x_N = 1,$$

and denote $\eta_{i,j}^n$ the numerical estimate of $\eta_i(t_n, x_j)$. The scheme, if upwind is used, reads:

$$(33) \quad \begin{aligned} \eta_{i,j}^{n+1} &= \eta_{i,j}^n + \frac{u_i \Delta t}{\Delta x} (\eta_{i,j}^n - \eta_{i,j-1}^n), & i = 1, 2, \quad j = 2, \dots, N; \\ \eta_{3,j}^{n+1} &= \eta_{3,j}^n + \frac{u_3 \Delta t}{\Delta x} (\eta_{3,j+1}^n - \eta_{3,j}^n), & j = 1, \dots, N-1. \end{aligned}$$

Here all $\eta_i(t, x_j)$ get updated except $\eta_{1,0}$, $\eta_{2,0}$ and $\eta_{3,N}$, whose information are determined from the kinetic boundary data ϕ_l and ϕ_r by the boundary layer equations, as we discuss below.

We first study the left boundary $x = 0$. Since by assumption of the Mach number $u_* > 0 > u_* - \sqrt{3T_*}$, at $x = 0$, $H^+ = \text{span}\{\chi_0, \chi_+\}$ while $\chi_- \in H^-$. The information restricted on H^- should be provided by

the left-going mode $\eta_3(x=1)$, while $\eta_{1,2}(x=0)$ need to be computed according to the layer equation. To be more specific, realizing

$$\begin{cases} \xi_{-,1} = \langle f^l|_{z=\infty}, \zeta_{-,1} \rangle = \langle f^l|_{z=\infty}, \chi_- \rangle = \frac{\sqrt{\rho_*}}{\sqrt{6T_*}} \langle f|_{z=\infty}, p_3 \rangle_{M_*} = \frac{\sqrt{\rho_*}}{\sqrt{6T_*}} \eta_3(x=0), \\ \xi_{+,1} = \langle f^l|_{z=\infty}, \zeta_{+,1} \rangle = \langle f^l|_{z=\infty}, \chi_0 \rangle = \frac{2\sqrt{\rho_*}}{\sqrt{6T_*}} \langle f|_{z=\infty}, p_1 \rangle_{M_*} = \frac{\sqrt{\rho_*}}{\sqrt{6T_*}} \eta_1(x=0), \\ \xi_{+,2} = \langle f^l|_{z=\infty}, \zeta_{+,2} \rangle = \langle f^l|_{z=\infty}, \chi_+ \rangle = \frac{\sqrt{\rho_*}}{\sqrt{6T_*}} \langle f^l|_{z=\infty}, p_2 \rangle_{M_*} = \frac{\sqrt{\rho_*}}{\sqrt{6T_*}} \eta_2(x=0), \end{cases}$$

we subtract the H^- mode provided by $\eta_3(x=0)$ from the layer equation:

$$(34) \quad \begin{cases} v\partial_z f^l = \mathcal{L}_* f^l, & (z, v) \in \mathbb{R}^+ \times \mathbb{R}, \\ f^l|_{z=x=0} = \phi_l(v) - \frac{\sqrt{\rho_*}}{\sqrt{6T_*}} \eta_{3,0}^{n+1} \chi_-(v), & v > 0. \end{cases}$$

The boundary layer equation (34) is then solved using the procedure in Theorem 2 for $f^l|_{z=\infty}$. From the solution of (34), we set:

$$(35) \quad \eta_{1,0}^{n+1} = \frac{3T_*}{\sqrt{6\rho_*}} \langle f^l|_{z=\infty}, \chi_0 \rangle, \quad \eta_{2,0}^{n+1} = \frac{\sqrt{6T_*}}{\sqrt{\rho_*}} \langle f^l|_{z=\infty}, \chi_+ \rangle.$$

The same procedure can be done for the right boundary at $x=1$ with $z = \frac{1-x}{\varepsilon}$ and $\tilde{v} = -v$. Here the sign is flipped, and thus $H^+ = \text{span}\{\chi_-\}$ and $H^- = \text{span}\{\chi_0, \chi_+\}$. Subtracting the H^- mode from the layer equation, we get

$$(36) \quad \begin{cases} \tilde{v}\partial_z f^r = \mathcal{L}_* f^r, & (z, v) \in \mathbb{R}^+ \times \mathbb{R}, \\ f^r|_{z=0(x=1)} = \phi_r(-v) - \frac{\sqrt{\rho_*}}{\sqrt{6T_*}} \eta_{1,N}^{n+1} \chi_+(v) - \frac{2\sqrt{\rho_*}}{\sqrt{6T_*}} \eta_{2,N}^{n+1} \chi_0(v), & v > 0. \end{cases}$$

We update η_3 at the right end accordingly from the solution of (36):

$$(37) \quad \eta_{3,N}^{n+1} = \frac{3T_*}{\sqrt{6\rho_*}} \langle f^r|_{z=\infty}, \chi_- \rangle.$$

Let us summarize the algorithm below.

4. COUPLING THE BGK AND THE EULER EQUATIONS

In this section we discuss the BGK equation coupled with the compressible Euler equation. For the conciseness of notation, we write:

$$(38) \quad \begin{cases} \partial_t F + v\partial_x F = \frac{1}{\varepsilon}(M[F] - F), & (t, x, v) \in \mathbb{R}^+ \times [-1, 1] \times \mathbb{R} \\ F(t, x = -1, v) = F_l(t, v), & v > 0 \\ F(t, x = 1, v) = F_r(t, v), & v < 0 \end{cases}$$

and assume in this section that $\varepsilon = 1$ in $x \in [0, 1]$ and $\varepsilon \ll 1$ in $x \in [-1, 0]$. Therefore the system is in kinetic regime on the right side and in fluid regime on the left side of $x=0$. Hence the boundary layer emerges at two locations: on the physical boundary at $x=1$ of the fluid regime and at the interface between the two regimes at $x=0$.

Compared to coupling linearized BGK with the acoustic limit, the coupling in the nonlinear setting is more challenging. First, the global Maxwellian no longer serves as a good approximation, and the linearization needs to be done locally around the local Maxwellian, which varies in time. This means at

Algorithm 1: Updating the computation of the acoustic limit from t_n to t_{n+1}

Data:

- 1 Kinetic boundary condition $\phi_l(v, t_{n+1})$ for $v > 0$ and $\phi_r(v, t_{n+1})$ for $v < 0$;
- 2 Solution at t_n : all $\eta_{i,j}^n$ for $i = 1, 2, 3$, and $j = 0, 1, \dots, N$.

Result: Solution at t_{n+1} : all $\eta_{i,j}^{n+1}$

Step I: Update $\eta_{i,j}^{n+1}$ in the interior according to (33);

Step II: Compute (34) and (36) using the procedure from Theorem 2 for $f^{l/r}|_{z=\infty}$;

Step III: Update boundary data:

for $i = 1, 2, 3$ **do**

if $u_i > 0$ **then**

 | Set $\eta_{i,0}$ according to (35);

else

 | Set $\eta_{i,N}$ according to (37);

end

end

every time step at each layer location, one conducts the linearization around local Maxwellian for the linear Knudsen layer equation, and sets up a set of basis function accordingly. Second, in the linearized case, the link between the acoustic modes and the projection of the boundary layer solution on $\text{Null}\mathcal{L}$ is explicit (35) and (37), making the computation relatively straightforward. In the nonlinear case, such connection is lost, and we thus need to explore for a new way to translate kinetic and fluid data.

Below we first review the numerical methods for each side (fluid and kinetic). The fluid equation will be computed using finite volume type method, and in the kinetic regime, we adopt the approach taken in [9], where an implicit scheme is applied but it is explicitly computable. The two regimes are then coupled through flux consistency.

We first unify the notations. Since flux is a crucial quantity in the numerical method, finite volume, instead of finite difference framework is used. Set $h = 1/N$ the spatial discretization, and $l = 1/M$ the velocity discretization. We divide the domain into $2N$ equally spaced cells, with N cells on each side of y -axis.

$$(39) \quad -1 = x_{1/2} < x_{3/2} < \dots < x_{N+1/2} = 0 < \dots < x_{2N-1/2} < x_{2N+1/2} = 1.$$

Also we restrict the velocity space to be $[-16, 16]$ during the numerical computation and divide it into $32M$ equal cells, with

$$(40) \quad -16 = v_0 < v_1 < \dots < v_{16M} = 0 < \dots < v_{32M-1} < v_{32M} = 16.$$

4.1. Computation in the fluid domain. In $x \in [-1, 0]$ we use finite volume method to compute the limiting compressible Euler equation (rewrite (3) in 1D):

$$\partial_t \mathcal{U} + \partial_x \mathcal{F}(\mathcal{U}) = 0,$$

with

$$\mathcal{U} = \begin{pmatrix} \rho \\ \rho u \\ E \end{pmatrix}, \quad \mathcal{F}(\mathcal{U}) = \begin{pmatrix} \rho u \\ \rho u^2 + \rho T \\ (E + \rho T)u \end{pmatrix},$$

where $E = \frac{1}{2}\rho u^2 + \frac{1}{2}\rho T$. Denote \mathcal{U}_i^n the numerical solution to the equation in cell $[x_{i-1/2}, x_{i+1/2}]$ at time t_n , and $\mathcal{F}_{i+1/2}^n$ the numerical flux at the cell boundary $x = x_{i+1/2}$. From time step t_n to t_{n+1} , we need to update for \mathcal{U}_i^{n+1} for all $i = 1, \dots, N$.

A standard conservative finite volume scheme reads

$$(41) \quad \mathcal{U}_i^{n+1} = \mathcal{U}_i^n - \frac{\Delta t}{h} (\mathcal{F}_{i+1/2}^n - \mathcal{F}_{i-1/2}^n).$$

This means we need to prepare $\mathcal{F}_{i-1/2}^n$ for all $i = 1, \dots, N + 1$.

For the flux term in the interior, we follow the standard finite volume method and choose the numerical flux that depends on the two neighboring cells only: $\mathcal{F}_{i+1/2}^n = F(\mathcal{U}_i^n, \mathcal{U}_{i+1}^n)$. In the computation we use the Roe flux. Take $\mathcal{F}_{i-1/2}$ for example, one has the formula (ignore the upper script for time step for the conciseness of the notation):

$$(42) \quad \mathcal{F}_{i-1/2} = \frac{1}{2} [\mathcal{F}(\mathcal{U}_{i-1}) + \mathcal{F}(\mathcal{U}_i)] - \frac{1}{2} |\hat{A}_{i-1/2}| (\mathcal{U}_i - \mathcal{U}_{i-1}), \quad i = 2, 3, \dots, N,$$

where $\hat{A}_{i-1/2}$ is the Jacobian of $\nabla_{\mathcal{U}} \mathcal{F}$:

$$\hat{A}_{i-1/2} = \begin{pmatrix} 0 & 1 & 0 \\ \frac{1}{2}(\gamma - 3)\hat{u}^2 & (3 - \gamma)\hat{u} & \gamma - 1 \\ \frac{1}{2}(\gamma - 1)\hat{u}^3 - \hat{u}\hat{H} & \hat{H} - (\gamma - 1)\hat{u}^2 & \gamma\hat{u} \end{pmatrix}$$

evaluated using averaged velocity \hat{u} , total specific enthalpy \hat{H} and sound speed \hat{c} :

$$\begin{cases} \hat{u} &= \frac{\sqrt{\rho_{i-1}}u_{i-1} + \sqrt{\rho_i}u_i}{\sqrt{\rho_{i-1}} + \sqrt{\rho_i}} \\ \hat{H} &= [(E_{i-1} + \rho_{i-1}T_{i-1})/\sqrt{\rho_{i-1}} + (E_i + \rho_iT_i)/\sqrt{\rho_i}] / [\sqrt{\rho_{i-1}} + \sqrt{\rho_i}] \\ \hat{c} &= \sqrt{2(\hat{H} - \frac{1}{2}\hat{u}^2)} \end{cases}.$$

At the two ends of the domain, $x_{1/2} = -1$ and $x_{N+1/2} = 0$, formula (42) is no longer valid, and we need to incorporate the boundary conditions. We defer the discussion to Section 4.3.

4.2. Computation in the kinetic region. In the kinetic region we update the full distribution function F by computing:

$$\partial_t F + v \partial_x F = M[F] - F, \quad (t, x, v) \in \mathbb{R}^+ \times [0, 1] \times \mathbb{R}.$$

With the pre-set discretization, we denote $F_{i,j}^n$ the numerical approximation at cell $[x_{i-1/2}, x_{i+1/2}]$ with velocity v_j given in (40) at time step t^n . For the computation we split the equation into two:

$$\begin{cases} \partial_t F + v \partial_x F = 0 \\ \partial_t F = M[F] - F \end{cases},$$

and correspondingly, the scheme reads:

$$(43) \quad \begin{cases} F_{i,j}^{n+1/2} &= F_{i,j}^n - \Delta t v_j (\partial_x F)_{i,j}^n, \\ F_{i,j}^{n+1} &= F_{i,j}^{n+1/2} - \frac{\Delta t}{\epsilon} (M_{i,j}^{n+1/2} - F_{i,j}^{n+1/2}). \end{cases}$$

In the first half step, we use the simple upwind method, namely:

$$\begin{cases} F_{i,j}^{n+1/2} = F_{i,j}^n - \frac{v_j \Delta t}{h} (F_{i,j}^n - F_{i-1,j}^n), & \text{for } i = N+2, \dots, 2N \text{ and } v_j > 0; \\ F_{i,j}^{n+1/2} = F_{i,j}^n - \frac{v_j \Delta t}{h} (F_{i+1,j}^n - F_{i,j}^n), & \text{for } i = N+1, \dots, 2N \text{ and } v_j < 0. \end{cases}$$

Here we set $F_{2N+1,j}^n = F_r(t_n, v_j)$ with $v_j < 0$ using the boundary conditions. This process leaves $F_{N+1,j}^{n+1/2}$ not updated for $v_j > 0$. To update it, the information from the interface boundary layer needs to be incorporated, and we leave it to the next section. In the second half, the only unknown is the Maxwellian function which could be updated using formula (8):

$$M_{i,j}^{n+1/2} = \frac{\rho_{i,j}^{n+1/2}}{(2\pi T_{i,j}^{n+1/2})^{1/2}} \exp\left(-\frac{(v - u_{i,j}^{n+1/2})^2}{2T_{i,j}^{n+1/2}}\right),$$

with its moments computed by taking moments of $F_{i,j}^{n+1/2}$

$$\begin{pmatrix} \rho^{n+1/2} \\ \rho^{n+1/2} u^{n+1/2} \\ E^{n+1/2} \end{pmatrix} = \sum_j \Delta v F_{ij}^{n+1/2} \begin{pmatrix} 1 \\ v_j \\ v_j^2/2 \end{pmatrix}.$$

4.3. Boundary flux. In this subsection we defines the numerical flux on the boundary cells proposed in [6] to connect the two regions. More specifically we need to compute $\mathcal{F}_{1/2}$ and $\mathcal{F}_{N+1/2}$ at the interfaces for the fluid side, and $F_{N+1,j}$ for $v_j > 0$ for the kinetic side. We first show the computation of $\mathcal{F}_{1/2}$ as an example.

According to the definition of the flux:

$$(44) \quad \mathcal{F}(\mathcal{U}) = \begin{pmatrix} \rho u \\ \rho u^2 + \rho T \\ (E + \rho T)u \end{pmatrix} = \int v \begin{pmatrix} 1 \\ v \\ |v|^2/2 \end{pmatrix} F dv,$$

it is easy to see that numerically to compute $\mathcal{F}_{1/2}$, one simply needs $F_{1/2}$.

Assume at time step t_n , the local Maxwellian is known, denoted as M_* , defined by ρ_* , u_* and T_* , then

$$(45) \quad F = M_* + \sqrt{M_*} f,$$

with f satisfying the Knudsen layer equation (ignoring higher order terms and perform coordinate stretching $z = \frac{x+1}{\epsilon}$):

$$(46) \quad \begin{cases} v \partial_z f = m_* - f, & (t, z, v) \in \mathbb{R}^+ \times [0, \infty] \times \mathbb{R} \\ f(z=0, v) = \frac{F - M_*}{\sqrt{M_*}}(t, x = -1, v) = \frac{F_l - M_*}{\sqrt{M_*}}, & v > 0 \end{cases}.$$

As analyzed in the previous section, $z = \infty$ corresponds to the end of the layer, which can be regarded as $x = x_{1/2} = -1$. At this point, $f \in \text{Null}\mathcal{L}$, meaning:

$$(47) \quad f = f_- + f_+, \quad \text{with} \quad f_- = \sum_{i=1}^{\nu_-} \xi_{-,i} \zeta_{-,i}, \quad f_+ = \sum_{i=1}^{\nu_0} \xi_{0,i} \zeta_{0,i} + \sum_{i=1}^{\nu_+} \xi_{+,i} \zeta_{+,i}$$

in charge of flow towards the wall and into the interior. Plugging (45) and (47) into (44), immediately, one gets:

$$(48) \quad \mathcal{F}_{1/2} = \int \left[M_* + \sqrt{M_*} f_- + \sqrt{M_*} f_+ \right] v \begin{pmatrix} 1 \\ v \\ |v|^2/2 \end{pmatrix} dv.$$

Here f_+ is in charge of the information getting into the interior from the physical boundary. It includes the positive modes provided by the Knudsen layer equation. The computation is given in Theorem 2. f_- is in charge of the information flowing out of the domain, and thus comes from the fluid side. We apply same algorithm as in [6] to compute the outgoing flow. Considering that f is the perturbation around the Maxwellian, one needs to find the fluctuation around the counterpart of the Maxwellian on the fluid side as well. Denote U_* the reference state (ρ_*, u_*, T_*) , and define the fluctuation term:

$$(49) \quad U_{\text{fluc}} = U_1 - U_* = (\rho_{\text{fluc}}, u_{\text{fluc}}, T_{\text{fluc}})^\top,$$

according to (14), the associated infinitesimal Maxwellian is:

$$(50) \quad m_{U_{\text{fluc}}} = \left[\frac{\rho_{\text{fluc}}}{\rho_*} + u_{\text{fluc}} \frac{v - u_*}{T_*} + \frac{T_{\text{fluc}}}{2T_*} \left(\frac{(v - u_*)^2}{T_*} - 1 \right) \right] \sqrt{M_*}.$$

We keep its projection onto the negative flows and use it to define f_- . Namely:

$$(51) \quad f_-(v) = \sum_{i=1}^{\nu_-} \xi_{-,i} \zeta_{-,i}, \quad \text{with} \quad \xi_{-,i} = \frac{\int v m_{U_{\text{fluc}}} \chi_{-,i} dv}{\int v |\chi_{-,i}|^2 dv}.$$

This finishes our computation for $\mathcal{F}_{1/2}$. In practice, we select, at t_n :

$$U_* = U_0^n + \frac{1}{2}(U_0^n - U_0^{n-1}),$$

and at the initial time step we set $U_* = U_0^1$.

We use the same derivation for computing the fluxes at the interface $x = x_{N+1/2} = 0$. Here note that the boundary layer is facing the left, and thus one sets $z = -\frac{x}{\varepsilon}$ and the velocity needs to flip the sign as well, meaning we compute the layer equation (46) with boundary condition:

$$(52) \quad f(z = 0, v) = \frac{F_{N+1}(-v) - M_*(-v)}{\sqrt{M_*(-v)}}.$$

The fluxes for the kinetic side is given by:

$$(53) \quad F_{N+1,j} = M_*(-v_j) + \sqrt{M_*(-v_j)} f(z = 0, -v_j), \quad \forall v_j > 0.$$

The algorithm is summarized in Algorithm 2.

Algorithm 2: Updating the coupled BGK-Euler system from t_n to t_{n+1}

Data:

- 1 Kinetic boundary condition $F_l(v, t_n)$ for $v > 0$ and $F_r(v, t_n)$ for $v < 0$;
- 2 Kinetic solution at t_n : F_{ij}^n for $i = N + 1, \dots, 2N$ and all j ;
- 3 Fluid solution at t_n : $\mathcal{U}_i^n = (\rho_i^n, \rho_i^n u_i^n, E_i^n)^T$ for $i = 1 \dots N$.

Result: Solution at t_{n+1} , including:

- 1 Kinetic solution at t_{n+1} : F_{ij}^{n+1} for $i = N + 1, \dots, 2N$ and all j ;
- 3 Fluid solution at t_{n+1} : \mathcal{U}_i^{n+1} for $i = 1, \dots, N$.

Step I: prepare boundary fluxes:

Compute (46), and use (48) for $\mathcal{F}_{1/2}^n$;

Compute (46) using the boundary condition in (52), and use (48) for $\mathcal{F}_{N+1/2}^n$, (53) for F_{N+1}^n ;

Step II: update fluids using (41);

Step III: update kinetics using (43).

5. NUMERICAL EXAMPLE

5.1. Acoustic limit. We demonstrate two numerical examples for computing the acoustic limit for the linearized BGK equation. In both cases, we set domain $x \in [0, 1]$ with two boundaries at $x = 0$ and $x = 1$. Compute the BGK equation directly as the reference solution using $\varepsilon = \{\frac{1}{32}, \frac{1}{64}, \frac{1}{128}, \frac{1}{256}\}$, with $h = 10^{-3}$ and $\Delta t = h/20$. Numerically we truncate the velocity domain for $v \in [-16, 16]$. The mesh is set such that h resolves the layer, which is of ε order, and Δt satisfies the CFL condition. To compute the acoustic limit we follow the algorithm presented in Section 3, and use sample grids using $h = 5 \times 10^{-3}$ and $\Delta t = h/10$.

For both examples, we present the numerical results for both the BGK reference solution with various of ε and the acoustic limit at $T = 0.1$, as presented in Figure 1 and 4, and we zoom in the layer to demonstrate the layer structure, as clearly seen in Figure 2 and 5. The convergence rate of the differentiation is calculated and shown in Figure 3 and 6 as a function of ε in log-log scale. Here the error for $\tilde{\rho}$ is computed using:

$$(54) \quad D_\rho = \|\tilde{\rho}_{\text{ref}} - \tilde{\rho}_{\text{Euler}}\|_{L_2([0.1, 0.9])}$$

with “ref” referring to the solution of the BGK equation, and “Euler” indicating the solution to the linearized Euler equation. D_u and D_T are computed similarly. It is shown that such differentiation converges algebraically fast.

Test1: Right boundary layer only. In the first test, we set the reference state as $\rho_* = 1, u_* = 2, T_* = 1/2$. Initial data and the left boundary conditions are placed both in $\text{Null}\mathcal{L}_*$ to avoid initial layer and the left boundary layer. This is a supersonic case and all boundary conditions for the acoustic limit should be placed at the left end. The initial and boundary conditions for the linearized BGK equation

are given:

$$\begin{cases} \text{Boundaries: } f_l(v, t) = (1+t)\chi_+ + (1+t)\chi_0 + (1+t)\chi_-, & f_r(v, t) = 0 \\ \text{Initial: } f_0(x, v) = \frac{1.25 \sin(2\pi x)}{\rho_*} + \frac{1.25 \sin(2\pi x)}{T_*}(v - u_*) + \frac{1.25 \sin(2\pi x)}{2T_*} \left(\frac{(v-u_*)^2}{T_*} - 1 \right) \end{cases} .$$

Correspondingly, we can compute for the initial and boundary conditions for the acoustic limit:

$$\begin{cases} \text{Boundaries: } \eta(x=0) = \left(-\frac{3T_*}{\sqrt{6\rho_*}}(1+t), \frac{\sqrt{6}}{\sqrt{\rho_*}}(1+t), -\frac{\sqrt{6}}{\sqrt{\rho_*}}(1+t) \right)^\top \\ \text{Initial: } \tilde{\rho}_0(x, v) = 1.25 \sin(2\pi x), \quad \tilde{u}_0(x, v) = 1.25 \sin(2\pi x), \quad \tilde{T}_0(x, v) = 1.25 \sin(2\pi x) \end{cases} .$$

Test2: Left boundary layer only. In the second test, we study the opposite of the previous example and set $\rho_* = 1, u_* = -2, T_* = 1/2$. It is still a supersonic case with all the modes propagating to the left. There will be no layer from the right side. The initial and boundary condition given to the BGK equation are:

$$(55) \quad \begin{cases} \text{Boundaries: } f_l(v, t) = 0, & f_r(v, t) = (1+t)\chi_+ + (1+t)\chi_0 + (1+t)\chi_- \\ \text{Initial: } f_0(x, v) = \frac{\sin(2\pi x)}{\rho_*} + \frac{\sin(2\pi x)}{T_*}(v - u_*) + \frac{\sin(2\pi x)}{2T_*} \left(\frac{(v-u_*)^2}{T_*} - 1 \right) \end{cases}$$

and correspondingly we have the data for the acoustic limit:

$$\begin{cases} \text{Boundaries: } \eta(x=1) = \left(-\frac{3T_*}{\sqrt{6\rho_*}}(1+t), \frac{\sqrt{6}}{\sqrt{\rho_*}}(1+t), -\frac{\sqrt{6}}{\sqrt{\rho_*}}(1+t) \right)^\top \\ \text{initial: } \tilde{\rho}_0(x, v) = \sin(2\pi x), \quad \tilde{u}_0(x, v) = \sin(2\pi x), \quad \tilde{T}_0(x, v) = \sin(2\pi x) \end{cases}$$

5.2. The Euler equation. This subsection is devoted to the coupling in the nonlinear setting. In Test 3, we assume ε is uniformly small, and the entire domain $[0, 1]$ is in the fluid regime, in this case we set the mesh size $h = 0.005$ and time step $\Delta t = 0.001$. In Test 4, we assume ε drastically changes from 1 to a small number at $x = 0.5$, and thus we compute the BGK equation in $[0, 0.5]$ and couple it with the fluid equation computed in $[0.5, 1]$. For the computation of the BGK equation, the velocity range is set as $v \in [-16, 16]$. To satisfy the CFL condition, we set the time step $\Delta t = h/20$.

For comparison we also compute the BGK equation over the whole domain as the reference solution with the mesh size $h = 0.001$ and $\Delta t = h/20$. The numerical velocity range is $v \in [-16, 16]$. In the fluid region, we use various of ε : $\varepsilon = \{\frac{1}{32}, \frac{1}{64}, \frac{1}{128}, \frac{1}{256}\}$ for comparison.

In Test 3, we expect boundary layers at the physical boundary $x = 0, 1$, and we compute the error term D_ρ defined by

$$D_\rho = \|\rho_{\text{ref}} - \rho_{\text{Euler}}\|_{L_2([0.1, 0.9])} .$$

D_u and D_T are computed similarly. In Test 4, we expect boundary layer at $x = 0.5$ at $x = 1$, and the error is defined by:

$$D_\rho = \|\rho_{\text{ref}} - \rho_{\text{Euler}}\|_{L_2([0.6, 0.9])} .$$

Test 3: Pure fluid over the entire domain. In this example ε is assumed to be small over the entire domain and fluid limit is accurate in $[0, 1]$. The initial and boundary conditions for the BGK equation are given as:

$$\begin{cases} \text{Boundaries: } F_l(v, t) = 0, & F_r(v, t) = 0 \\ \text{Initial: } F_0(x, v) = \frac{1}{\sqrt{2\pi}} \exp\left(\frac{(v-0.1)^2}{2}\right) \end{cases}$$

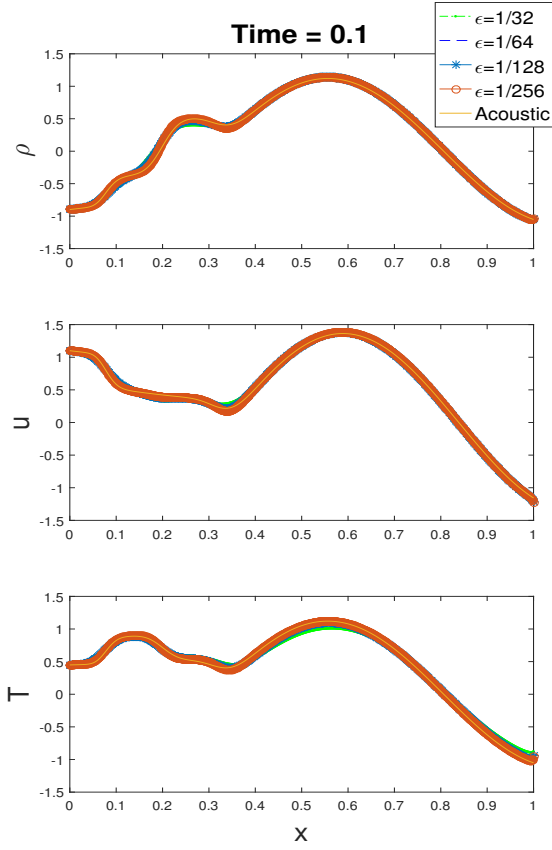


FIGURE 1. Test 1: Solution at $T = 0.1$.

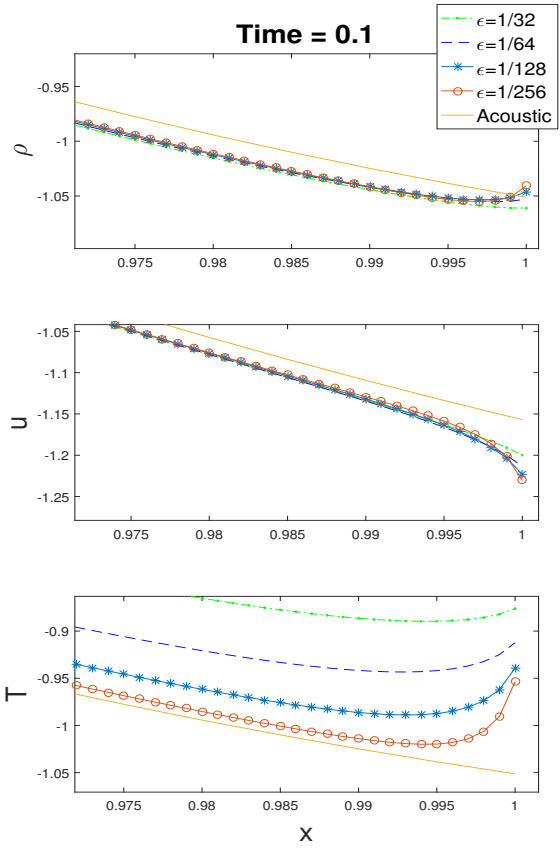


FIGURE 2. Test 1: Boundary layer zoomed around $x = 1$.

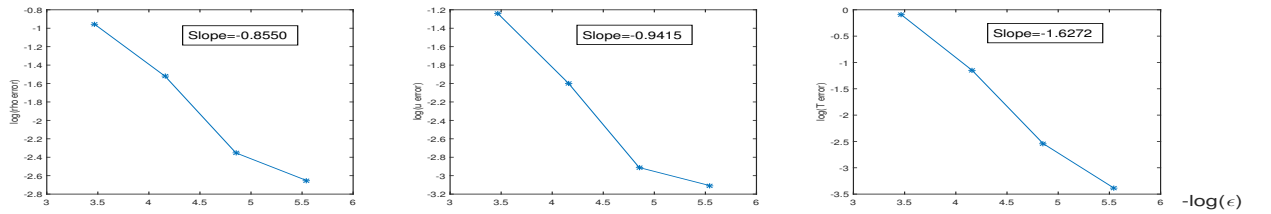


FIGURE 3. Test 1: Error D_ρ , D_u and D_T as functions of ϵ in log-log scale.

The initial condition is so set to avoid initial layer. Correspondingly we obtain the initial condition for the Euler equation:

$$\text{Initial: } \rho = 1, \quad u = 0.1, \quad T = 1.$$

We plot the solution profiles at $T = 0.1$ and the zoom-in at the layer in Figure 7, 8. Figure 9 presents the convergence rate of the differentiation.

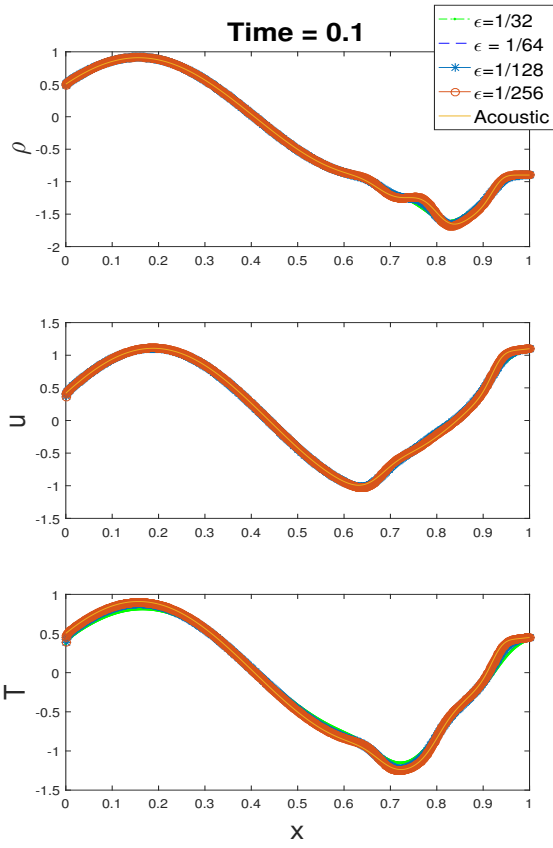


FIGURE 4. Test 2: Solution at $T = 0.1$.

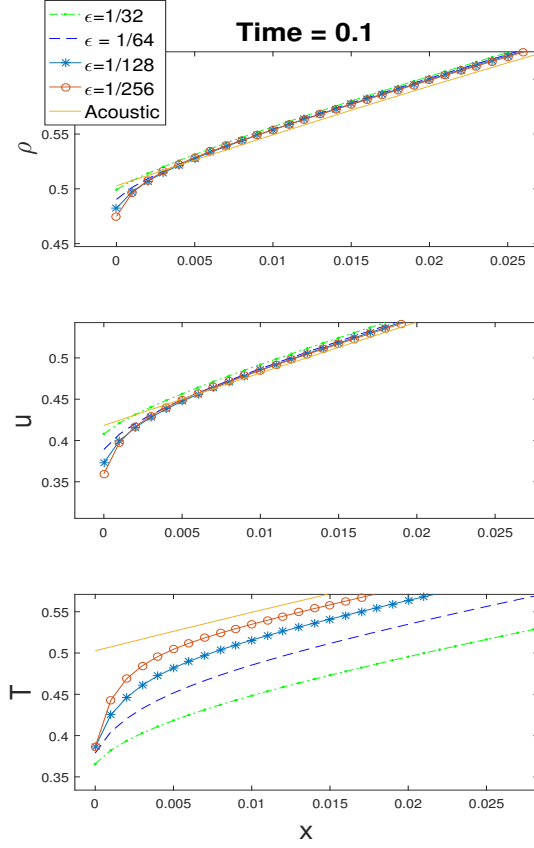


FIGURE 5. Test 2: Boundary layer zoomed around $x = 0$.

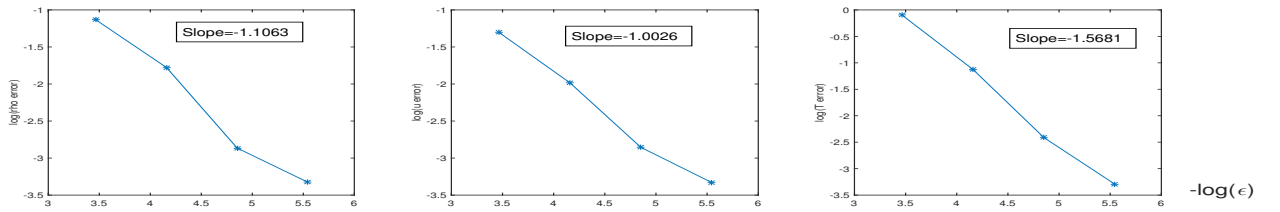
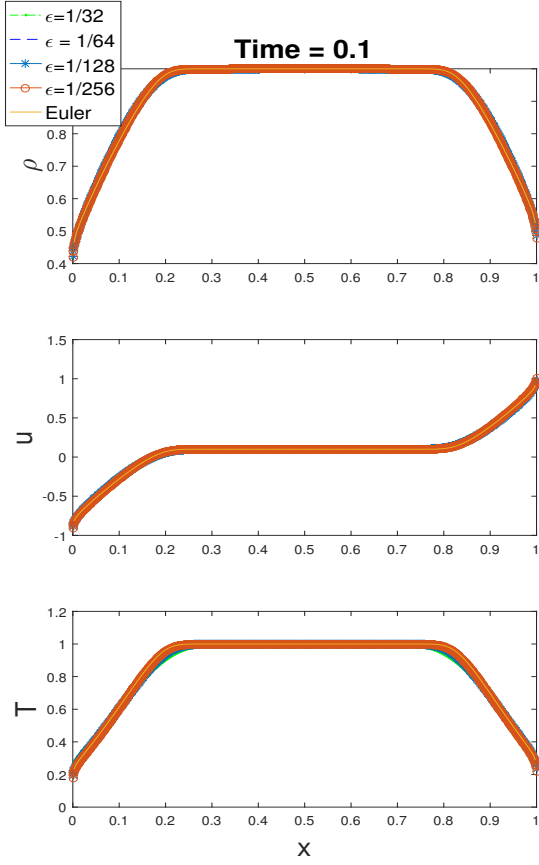
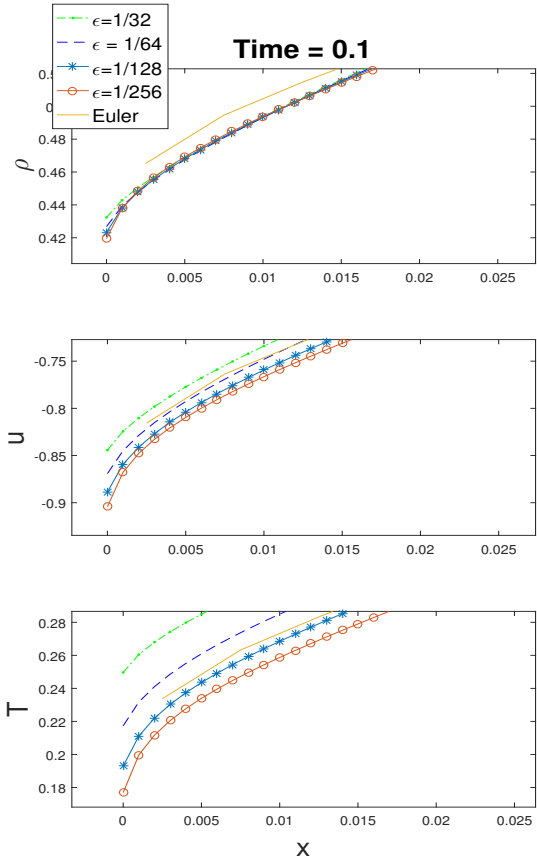
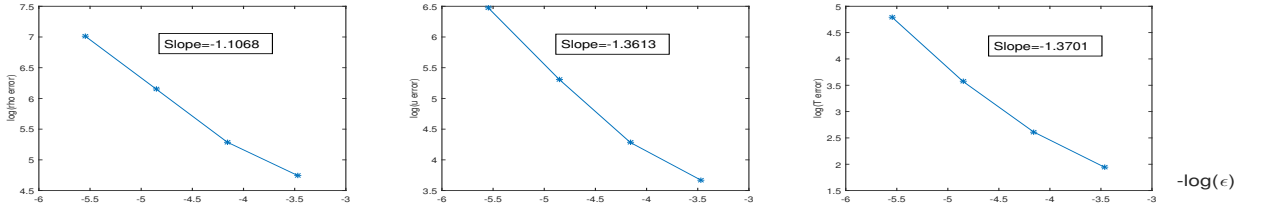


FIGURE 6. Test 2: Error D_ρ , D_u and D_T as functions of ϵ in log-log scale.

Test4: coupling the Euler and the BGK equation. In this test the fluid limit holds true in the right part of the domain, and we compute the Euler equation in $x \in [0.5, 1]$, and couple it with the BGK equation computed in $x \in [0, 0.5]$. Two layers need to be taken care of: at the physical boundary $x = 1$ and at the interface $x = 0.5$. The computation is done according to Algorithm 2.


 FIGURE 7. Test 3: Solution at $T = 0.1$

 FIGURE 8. Test 3: Boundary layer zoomed around $x = 0$.

 FIGURE 9. Test 3: Error D_ρ , D_u and D_T as functions of ε in log-log scale.

The initial and boundary conditions for the BGK equation are given as:

$$(56) \quad \begin{cases} \text{Boundaries: } F_l(x, v) = 0, & F_r(x, v) = 0 \\ \text{Initial: } F_0(x, v) = \begin{cases} \frac{1}{\sqrt{2\pi}} e^{-(v-0.1)^2/2}, & x > 1/2; \\ \frac{1}{\sqrt{4\pi}} e^{-(v-0.2)^2/4}, & x \leq 1/2. \end{cases} \end{cases}$$

Correspondingly one has the macroscopic quantities for the Euler equation at the initial time step:

$$\rho = \begin{cases} 1, & x \leq 1/2; \\ 2, & x > 1/2. \end{cases} \quad u = \begin{cases} 0.1, & x \leq 1/2; \\ 0.2, & x > 1/2. \end{cases} \quad T = \begin{cases} 1, & x \leq 1/2; \\ 2, & x > 1/2. \end{cases}$$

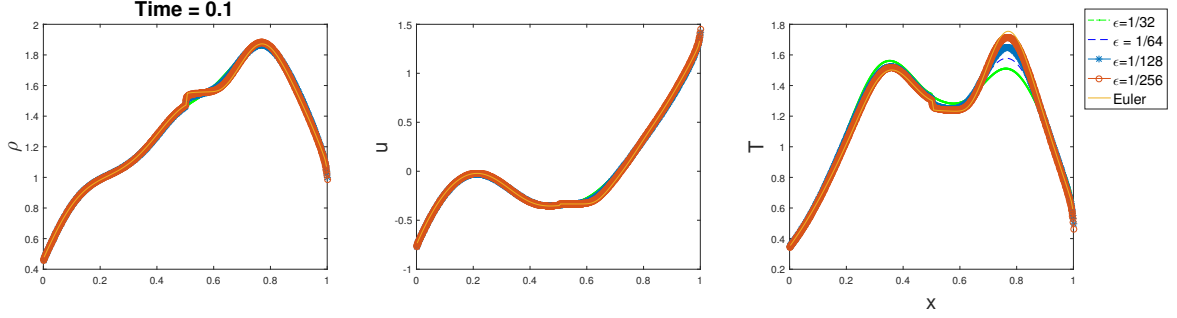


FIGURE 10. Test 4: solution at $T = 0.1$.

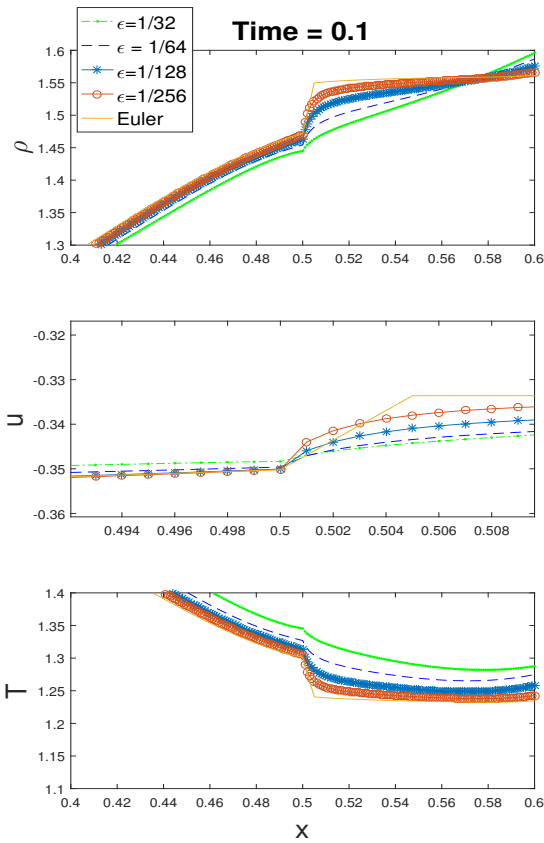


FIGURE 11. Test 4: Interfacial at $x = 0.5$.

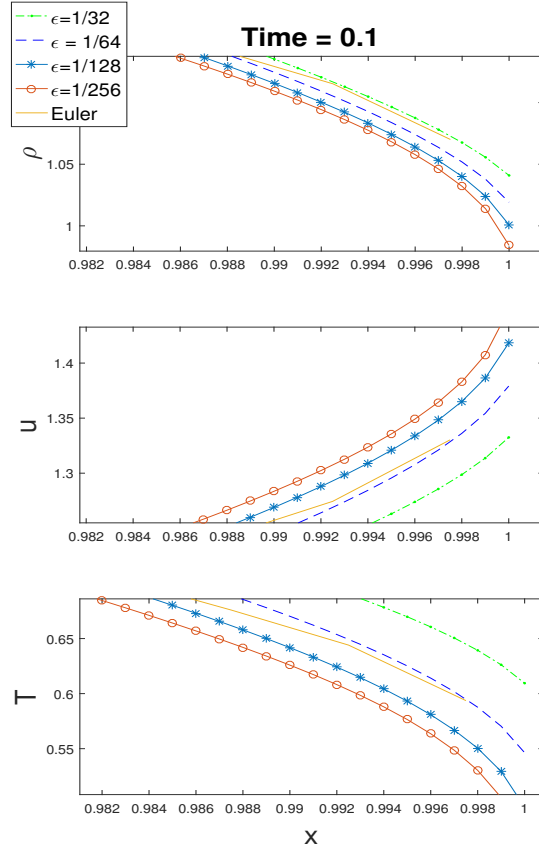


FIGURE 12. Test 4: Boundary layer zoomed in at $x = 1$.

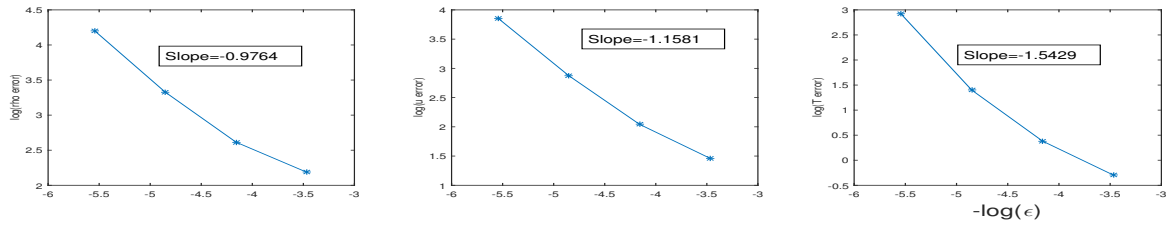


FIGURE 13. Test 4: Error D_ρ , D_u and D_T as functions of ϵ in log-log scale.

We compute the system up to time $T = 0.1$. Figure 10 shows the profiles of the solutions. Figure 11 and Figure 12 show the boundary layer at the interface and the physical boundary at $x = 1$ respectively. In Figure 13 we present the convergence in ϵ in log-log scale.

REFERENCES

1. Kazuo Aoki, Yoshio Sone, and Tatsuo Yamada, *Numerical analysis of gas flows condensing on its plane condensed phase on the basis of kinetic theory*, Physics of Fluids A: Fluid Dynamics **2** (1990), no. 10, 1867–1878.
2. C. Bardos, F. Golse, and D. Levermore, *Fluid dynamic limits of kinetic equations. I. Formal derivations*, J. Stat. Phys. **63** (1991), 323–344.
3. Claude Bardos, Russel E Caflisch, and Basil Nicolaenko, *The milne and kramers problems for the boltzmann equation of a hard sphere gas*, Communications on pure and applied mathematics **39** (1986), no. 3, 323–352.
4. M. Bennoune, M. Lemou, and L. Mieussens, *Uniformly stable numerical schemes for the Boltzmann equation preserving the compressible Navier-Stokes asymptotics*, J. Comput. Phys. **227** (2008), 3781–3803.
5. Alain Bensoussan, Jacques L. Lions, and George C. Papanicolaou, *Boundary layers and homogenization of transport processes*, Publications of the Research Institute for Mathematical Sciences **15** (1979), no. 1, 53–157.
6. Christophe Besse, Saja Borghol, Thierry Goudon, Ingrid Lacroix-Violet, and Jean-Paul Dudon, *Hydrodynamic regimes, knudsen layer, numerical schemes: definition of boundary fluxes*, Advances in Applied Mathematics and Mechanics **3** (2011), no. 5, 519–561.
7. J. F. Bourgat, P. Le Tallec, B. Perthame, and Y. Qiu, *Coupling Boltzmann and Euler equations without overlapping*, Domain decomposition methods in science and engineering, vol. 157, AMS, 1994, pp. 377–398.
8. F. Coron, F. Golse, and C. Sulem, *A classification of well-posed kinetic layer problems*, Comm. Pure Appl. Math. **41** (1988), 409–435.
9. F Coron and B Perthame, *Numerical passage from kinetic to fluid equations*, SIAM Journal on Numerical Analysis **28** (1991), no. 1, 26–42.
10. Nicolas Crouseilles, Pierre Degond, and M Lemou, *Hybrid kinetic/fluid models for nonequilibrium systems*, Comptes Rendus Mathematique **336** (2003), no. 4, 359–364.
11. P. Degond and M. Schmeiser, *Kinetic boundary layers and fluid-kinetic coupling in semiconductors*, Transport Theory Statist. Phys. **28** (1999), no. 1, 31–55.
12. Pierre Degond, Giacomo Dimarco, and Luc Mieussens, *A moving interface method for dynamic kinetic–fluid coupling*, Journal of Computational Physics **227** (2007), no. 2, 1176–1208.
13. Pierre Degond and Shi Jin, *A smooth transition model between kinetic and diffusion equations*, SIAM journal on numerical analysis **42** (2005), no. 6, 2671–2687.
14. G. Dimarco and L. Pareschi, *Exponential Runge-Kutta methods for stiff kinetic equations*, SIAM Journal on Numerical Analysis **49** (2011), no. 1, 2057–2077.
15. ———, *Numerical methods for kinetic equations*, Acta Numer. **23** (2014), 369–520.
16. F. Filbet and S. Jin, *A class of asymptotic-preserving schemes for kinetic equations and related problems with stiff sources*, J. Comput. Phys. **229** (2010), 7625–7648.
17. F. Golse and A. Klar, *A numerical method for computing asymptotic states and outgoing distributions for kinetic linear half-space problems*, J. Stat. Phys. **80** (1995), no. 5–6, 1033–1061.
18. François Golse, Shi Jin, and C David Levermore, *The convergence of numerical transfer schemes in diffusive regimes i: Discrete-ordinate method*, SIAM journal on numerical analysis **36** (1999), no. 5, 1333–1369.
19. ———, *A domain decomposition analysis for a two-scale linear transport problem*, ESAIM: Mathematical Modelling and Numerical Analysis **37** (2003), no. 6, 869–892.
20. François Golse and Axel Klar, *A numerical method for computing asymptotic states and outgoing distributions for kinetic linear half-space problems*, Journal of statistical physics **80** (1995), no. 5–6, 1033–1061.
21. S. Jin, *Efficient asymptotic-preserving (AP) schemes for some multiscale kinetic equations*, SIAM J. Sci. Comput. **21** (1999), 441–454.
22. ———, *Asymptotic preserving (AP) schemes for multiscale kinetic and hyperbolic equations: a review*, Riv. Mat. Univ. Parma **3** (2012), 177–216.
23. A. Klar, *Convergence of alternating domain decomposition schemes for kinetic and aerodynamic equations*, Math. Methods Appl. Sci. **18** (1995), no. 8, 649–670.

24. Axel Klar, *Domain decomposition for kinetic problems with nonequilibrium states*, Eur. J. Mech. B **15** (1996), no. 2, 203–216.
25. Edward W. Larsen, *On numerical solutions of transport problems in the diffusion limit*, Nuclear Science and Engineering **83** (1983), no. 1, 90–99.
26. Mohammed Lemou and Florian Méhats, *Micro-macro schemes for kinetic equations including boundary layers*, SIAM Journal on Scientific Computing **34** (2012), no. 6, B734–B760.
27. Q. Li and L. Pareschi, *Exponential Runge-Kutta for the inhomogeneous Boltzmann equations with high order of accuracy*, J. Comput. Phys. **259** (2014), 402–420.
28. Qin Li, Jianfeng Lu, and Weiran Sun, *Diffusion approximations and domain decomposition method of linear transport equations: Asymptotics and numerics*, Journal of Computational Physics **292** (2015), 141167.
29. ———, *A convergent method for linear half-space kinetic equations*, ESAIM: Mathematical Modelling and Numerical Analysis **51** (2017), no. 5, 1583–1615.
30. ———, *Half-space kinetic equations with general boundary conditions*, Mathematics of Computation **86** (2017), 1269–1301.
31. E. Wild, *On Boltzmann's equation in the kinetic theory of gases*, Mathematical Proceedings of the Cambridge Philosophical Society **47** (1951), 602 – 609.

APPENDIX A. NUMERICAL SCHEME FOR HALF-SPACE KINETIC EQUATIONS

In the appendix we present the numerical scheme for half-space kinetic equations. The numerical method presented in [29, 30] only considers a fixed reference state $\rho_* = 1, T_* = 1/2$, while the approximation method we developed in this paper involves changing reference state, thus we need to generalize the numerical methods for all reference states.

A.1. Numerical method for boundary layer equation. In this subsection, we focus on the numerical method for the half-space problems under the linearized BGK operator. This is a similar case of the algorithm proposed in the previous work [29, 30]. Consider the half-space problem, here we shift the original equation by u_* ,

$$(57) \quad \begin{cases} (v + u_*)\partial_x f + \mathcal{L}f = 0, \\ f(0, v) = f_0(v), & v + u_* > 0, \\ f(x, v) \rightarrow \theta_\infty \in H^0 \oplus H^+, & x \rightarrow \infty \end{cases}$$

To solve the infinite domain problem, we use a spectral discretization for the v -variable. In general the solution may exhibit singularity like jumps at $v = -u_*$. Hence we use an even-odd decomposition of the distribution function to avoid the Gibbs phenomena and ensure the accuracy. Here we define the shifted even and odd parts of a function as

$$(58) \quad f^E(v) = \frac{f(v) + f(-2u_* - v)}{2}, \quad f^O(v) = \frac{f(v) - f(-2u_* - v)}{2}$$

such that $f = f^E + f^O$. Due to the symmetry, it suffices to discretize the function f^E and f^O for $v \in (-u_*, \infty)$ and then extend the functions to the whole interval $v \in (-\infty, \infty)$. In other words, we use the half-space general weight Hermite polynomials as basis functions. The construction of the basis functions will be given in the next subsection. Then the even-odd extension is given by

$$(59) \quad B_m^E(v + u_*) = \begin{cases} B_m(v + u_*)/\sqrt{2}, & v > -u_* \\ B_m(-v - u_*)/\sqrt{2}, & v < -u_* \end{cases} \quad B_m^O(v + u_*) = \begin{cases} B_m(v + u_*)/\sqrt{2}, & v > -u_* \\ -B_m(-v - u_*)/\sqrt{2}, & v < -u_* \end{cases}$$

where $B_m(v + u_*)$ are the general weight Hermite polynomials on $(-u_*, \infty)$ satisfying

$$\int_{-u_*}^{\infty} B_n(v + u_*)B_m(v + u_*)e^{-(v+u_*)^2/2T} dv = \int_0^{\infty} B_n(v)B_m(v)e^{-v^2/2T} dv = \delta_{nm}$$

finally the basis functions P_n are obtained by multiplying these functions by the square root of the Maxwellian:

$$(60) \quad P_{2n-1}(v + u_*) = B_{n-1}^O(v + u_*)e^{-(v+u_*)^2/2T}$$

$$(61) \quad P_{2n}(v + u_*) = B_{n-1}^E(v + u_*)e^{-(v+u_*)^2/2T}$$

For the stability of the numerical method, we first solve a damped version of and then recover the solution to the original equation. Note that after the shift the basis function of the null space of \mathcal{L}_* is given by

$$(62) \quad \begin{cases} \chi_0(v) = \frac{1}{\sqrt{6}}\left(\frac{v^2}{T_*} - 3\right)\sqrt{M_{[0, T_*]}}, \\ \chi_+(v) = \frac{1}{\sqrt{6}}\left(\sqrt{\frac{3}{T_*}}v + \frac{v^2}{T_*}\right)\sqrt{M_{[0, T_*]}}, \\ \chi_-(v) = \frac{1}{\sqrt{6}}\left(\sqrt{\frac{3}{T_*}}v - \frac{v^2}{T_*}\right)\sqrt{M_{[0, T_*]}}, \end{cases}$$

The damped equation is given by

$$(63) \quad \begin{cases} (v + u_*)\partial_x f + \mathcal{L}_d f = 0, \\ f(0, v) = f_0(v), \end{cases} \quad v + u_* > 0,$$

where

$$(64) \quad \begin{aligned} \mathcal{L}_d f &= \mathcal{L}f + \sum_{k=1}^{v_+} \alpha(v + u_*)\chi_+ \langle (v + u_*)\chi_+, f \rangle + \sum_{k=1}^{v_0} \alpha(v + u_*)\chi_0 \langle (v + u_*)\chi_0, f \rangle \\ &+ \sum_{k=1}^{v_-} \alpha(v + u_*)\chi_- \langle (v + u_*)\chi_-, f \rangle + \sum_{k=1}^{v_0} \alpha(v + u_*)\mathcal{L}^{-1}((v + u_*)\chi_0) \langle (v + u_*)\mathcal{L}^{-1}((v + u_*)\chi_0) \rangle \end{aligned}$$

The well-posedness of this equation is proved in Proposition 3.2 [29], which verifies the inf-sup condition of the variational formulation. We approximate the even and odd parts of the distribution functions by

$$(65) \quad f^E(x, v) = \sum_{n=1}^N a_n^E(x) P_n^E(v), \quad f^O(x, v) = \sum_{n=1}^{N+1} a_n^O P_n^O(v)$$

Substituting the approximation into and applying Galerkin method, we obtain the equation for the coefficients which reads

$$(66) \quad A\partial_x \vec{a} = B\vec{a}$$

where

$$(67) \quad A_{ij} = \langle v P_i, P_j \rangle, \quad B_{ij}^E = \langle \mathcal{L}_d P_i, P_j \rangle$$

After diagonalizing the equation into a generalized eigenvalue problem, we obtain a system of $2N + 1$ ODE reads

$$(68) \quad \partial_x \vec{b} = V\vec{b}$$

with $A^{-1}B = XVX^{-1}$ and $b = Xa$. V is a diagonal matrix. The solution of the ODE tell us that we need $2N + 1$ boundary conditions to determine \vec{b} . The boundary conditions are of two kinds. The first is given by the Dirichlet boundary condition. Note that the boundary condition only provides data at $v > -u_*$, we only get N conditions for \vec{b} . The remaining conditions come from the requirement that $f \rightarrow \theta_\infty \in H^0 \oplus H^+$, this means \vec{a} can not be exponential increasing. Hence positive eigenvalue corresponds to 0 coefficient of \vec{b} . It is proved in Proposition 4.6 [29] that there are exactly N positive eigenvalues and 1 zero eigenvalue of the generalized eigenvalue. We obtain enough conditions to determine $\vec{a} = X\vec{b}$.

Once we obtain the solution of the damped equation, we can explicitly construct solutions to the undamped equation as stated in Theorem 2. Specifically, let g_+ be the solution to (47) with boundary conditions given by χ_+ :

$$g_+|_{x=0} = \chi_+, \quad v + u_* > 0$$

Similarly, denote g_0 as the solution to (47) where the incoming boundary data is given by χ_0 . Let C be the block matrix defined by

$$(69) \quad C = \begin{pmatrix} C_{++} & C_{+0} \\ C_{0+} & C_{00} \end{pmatrix}$$

where

$$\begin{aligned} C_{++} &= \langle (v + u_*)\chi_+, g_+ \rangle|_{x=0}, & C_{+0} &= \langle (v + u_*)\chi_+, g_0 \rangle|_{x=0} \\ C_{0+} &= \langle (v + u_*)\chi_0, g_+ \rangle|_{x=0}, & C_{00} &= \langle (v + u_*)\chi_0, g_0 \rangle|_{x=0} \end{aligned}$$

Define the coefficient vector $\eta = (\eta_+, \eta_1)^T$ such that

$$(70) \quad C\eta = U_f$$

where $U_f = (u_+, u_0)$ with $u_+ = \langle (v + u_*)\chi_+, f \rangle_{x=0}$ and $u_0 = \langle (v + u_*)\chi_0, f \rangle_{x=0}$.

In fact, C is invertible and hence (66) is uniquely solvable, moreover,

$$(71) \quad f_\phi = f - \sum_{k=1}^{v_+} \eta_+(g_+ - \chi_+) - \sum_{k=1}^{v_0} \eta_0(g_0 - \chi_0)$$

is the unique solution to the half-space equation

$$(72) \quad (v + u_*)\partial_x f + \mathcal{L}f = 0$$

$$(73) \quad f|_{x=0} = \phi(v) \quad v + u_* > 0$$

Moreover, the end state $f_{\phi, \infty}$ is given by

$$f_{\phi, \infty} = \sum_{k=1}^{v_+} \eta_+ \chi_+ + \sum_{k=1}^{v_0} \eta_0 \chi_0$$

In sum, we use the algorithm described above to obtain the solution of the half-space kinetic equation and then use the algorithm described in previous section to deal with the coupling problems.

A.2. General half-space Hermite polynomials. As described in previous subsection, to generalized the algorithm for general reference state, we can see the key is to generalized the half-space Hermite polynomials. Then the Galerkin method remains the same.

The basis functions is constructed using the half-space Hermite polynomials, which are orthogonal polynomials defined on the positive half v -axis with the weight function $e^{-v^2/2T}$: $\{B_n(v), v > 0\}$ such that each $B_n(v)$ is a polynomial of order n and

$$(74) \quad \int_0^\infty B_m(v)B_n(v)e^{-v^2/2T}dv = \delta_{nm}$$

The orthogonal polynomials can be constructed using three tern recursion formula, for the derivation one can see the details in appendix.

The basis function we need are either odd or even with respect to $v = u$, thus we shift B_n by $-u$ and make even-odd extension

$$(75) \quad B_n^E(v) = \begin{cases} B_n(v+u)/\sqrt{2}, & v > -u; \\ B_n(-v-u)/\sqrt{2}, & v < -u. \end{cases}$$

$$(76) \quad B_n^O(v) = \begin{cases} B_n(v+u)/\sqrt{2}, & v > -u; \\ -B_n(-v-u)\sqrt{2}, & v < -u. \end{cases}$$

The $(2N+1) \times (2N+1)$ matrices are given by

$$A_{ij} = \int_{\mathbb{R}} (v+u)P_iP_jdv, \quad B_{ij} = - \int_{\mathbb{R}} P_i\mathcal{L}_dP_jdv$$

A can be obtained by the recurrence relation. For matrix B , recall that

$$(77) \quad \mathcal{L}_df = \mathcal{L}f + \sum_{k=1}^{v_+} \alpha(v+u)\chi_+ \langle (v+u)\chi_+, f \rangle + \sum_{k=1}^{v_0} \alpha(v+u)\chi_0 \langle (v+u)\chi_0, f \rangle \\ + \sum_{k=1}^{v_-} \alpha(v+u)\chi_- \langle (v+u)\chi_-, f \rangle + \sum_{k=1}^{v_0} \alpha(v+u)\mathcal{L}^{-1} \langle (v+u)\chi_0, (v+u)\mathcal{L}^{-1} \langle (v+u)\chi_0, f \rangle \rangle$$

All the integrals involved in calculating B can be obtained by using the Gaussian quadrature. To see this, we take χ_0 as an example, all other integrals can be treated in the same way. We firstly split the integral into two parts

$$\int_{-\infty}^{\infty} P_{2i}\chi_0dv = \int_{-u}^{\infty} P_{2i}\chi_0dv + \int_{-\infty}^{-u} P_{2i}\chi_0dv$$

Note that P_{2i} , on each side of $-u$, is i -th order polynomial product with $\exp(-\frac{(v+u)^2}{4T})$ while χ_0 is a quadratic function multiplied with a different weight function $\exp(-v^2/4T)$. The two Gaussians that entered at different locations could be combined, and the numerical integral is exact once the correct Gaussian quadrature is adopted:

$$(78) \quad \int_{-u}^{\infty} P_n(v)\chi_0(v)dv = \frac{1}{\sqrt{2}} \int_{-u}^{\infty} B_n(v+u)\chi_0e^{-\frac{(v+u)^2+v^2}{4T}}dv \\ = \frac{1}{\sqrt{2}} \int_0^{\infty} B_n(v)\chi_0(v-u)e^{-\frac{2v^2-2vu+u^2/2+u^2/2}{4T}}dv = \frac{1}{\sqrt{2}}e^{-u^2/8T} \int_0^{\infty} B_n(v-u)\chi_0(v-u)e^{-\frac{(v-u/2)^2}{2T}}dv$$

Similarly, we have the integration from the negative part,

$$\int_{-\infty}^{-u} P_n\chi_0dv = \frac{1}{\sqrt{2}} \int_{-\infty}^{-u} B_n(v+u)\chi_0e^{-\frac{(v+u)^2+v^2}{4T}}dv = \frac{1}{\sqrt{2}}e^{-u^2/8T} \int_0^{\infty} B_n(-v-u)\chi_0(-v)e^{-\frac{(v+u/2)^2}{2T}}dv$$

Thus these integrals can be obtained by using the Gaussian quadrature of the weight $e^{-(v-u/2)^2/2T}$ and $e^{-(v+u/2)^2/2T}$ respectively.

A.3. Derivation of recurrence relation. Here we derive the half-space orthogonal polynomials with weight $\exp((v-u)^2/2T)$. The zeroth order is

$$B_0 = \frac{1}{\sqrt{m_0}}, \quad m_0 = \frac{\sqrt{\pi}}{2} \left(1 + \operatorname{erf}\left(\frac{u}{2T}\right)\right)$$

Set the recurrence relation for the higher order polynomials as

$$(79) \quad \sqrt{\beta_{n+1}}B_{n+1} = (v - \alpha_n)B_n - \sqrt{\beta_n}B_{n-1}$$

we aim to derive the formula for β_n and α_n . Actually

$$(80) \quad \begin{cases} \beta_{n+1} = 2Tn + T - \beta_n + u\alpha_n - \alpha_n^2 \\ \alpha_{n+1} = \frac{T}{\beta_{n+1}} \sum_{k=0}^n \alpha_k - \alpha_n + u \end{cases}$$

with $\alpha_0 = m_1/m_0$, $\beta_0 = 0$ where m_i , $i=0,1$ are moments of the Gaussian:

$$(81) \quad m_i = \int_0^\infty v^i e^{-(v-u)^2/2T} dv$$

Now we start the derivation. From the recurrence relation we get

$$\alpha_n = \int_0^\infty v B_n^2 e^{-\frac{(v-u)^2}{2T}} dv, \quad \sqrt{\beta_{n+1}} = \int_0^\infty v B_n B_{n+1} e^{-\frac{(v-u)^2}{2T}} dv$$

By the Christoffel-Darboux identity

$$(82) \quad \sum_{k=0}^n B_k^2 = \sqrt{\beta_{n+1}}(B'_{n+1}B_n - B_{n+1}B'_n)$$

By integrating this identity with the weight we get

$$n+1 = \sqrt{\beta_{n+1}} \int_0^\infty B'_{n+1}B_n e^{-\frac{(v-u)^2}{2T}} dv$$

Note that

$$\sqrt{\beta_{n+1}}B'_{n+1} = B_n + (v - \alpha_n)B'_n - \sqrt{\beta_n}B'_{n-1}$$

We have

$$\begin{aligned} n+1 &= 1 + \int_0^\infty (v - \alpha_n)B'_n B_n e^{-\frac{(v-u)^2}{2T}} dv = 1 + \int_0^\infty v B'_n B_n e^{-\frac{(v-u)^2}{2T}} dv \\ n &= - \int_0^\infty \frac{1}{2}(B_n)^2 \left[v e^{-\frac{(v-u)^2}{2T}} \right]' dv = - \int_0^\infty \frac{1}{2}(B_n)^2 \left[e^{-\frac{(v-u)^2}{2T}} - \frac{v-u}{T} v e^{-\frac{(v-u)^2}{2T}} \right] dv \\ &= -\frac{1}{2} + \int_0^\infty \frac{1}{2T} v^2 B_n^2 e^{-\frac{(v-u)^2}{2T}} dv - \frac{1}{2T} u \alpha_n \end{aligned}$$

Note that

$$vB_n = \sqrt{\beta_{n+1}}B_{n+1} + \alpha_n B_n + \sqrt{\beta_n}B_{n-1}$$

we get

$$v^2 B_n^2 = \sqrt{\beta_{n+1}}vB_{n+1}B_n + v\alpha_n B_n^2 + v\sqrt{\beta_n}B_n B_{n-1}$$

Therefore,

$$\begin{aligned} n &= -\frac{1}{2} + \frac{1}{2T}(\beta_{n+1} + \alpha_n^2 + \beta_n - u\alpha_n) \\ \beta_{n+1} &= 2Tn + T - \beta_n + u\alpha_n - \alpha_n^2 \end{aligned}$$

Next we multiply the identity with v and then integrate to obtain

$$\begin{aligned} \sum_{k=0}^n \alpha_k &= \sqrt{\beta_{n+1}} \int_0^\infty v B'_{n+1} B_n e^{-\frac{(v-u)^2}{2T}} dv \\ &= \sqrt{\beta_{n+1}} \left(\int_0^\infty \frac{v^2}{T} B_{n+1} B_n e^{-\frac{(v-u)^2}{2T}} - \int_0^\infty \frac{vu}{T} B_{n+1} B_n e^{-\frac{(v-u)^2}{2T}} dv \right) = \frac{\beta_{n+1}}{T} (\alpha_n + \alpha_{n+1} - u) \\ \alpha_{n+1} &= \frac{T}{\beta_{n+1}} \sum_{k=0}^n \alpha_k - \alpha_n + u \end{aligned}$$

MATHEMATICS DEPARTMENT, UNIVERSITY OF WISCONSIN-MADISON, 480 LINCOLN DR., MADISON, WI 53705 USA.

E-mail address: `hchen463@wisc.edu`

MATHEMATICS DEPARTMENT, UNIVERSITY OF WISCONSIN-MADISON, 480 LINCOLN DR., MADISON, WI 53705 USA.

E-mail address: `qinli@math.wisc.edu`

DEPARTMENT OF MATHEMATICS, DEPARTMENT OF PHYSICS, AND DEPARTMENT OF CHEMISTRY, DUKE UNIVERSITY, BOX 90320, DURHAM NC 27708, USA

E-mail address: `jianfeng@math.duke.edu`